Endoleak detection after endovascular aortic aneurysm repair utilizing dynamic, time-resolved computed tomography angiography

Ph.D. Thesis

Márton Tibor Berczeli

Károly Rácz Doctoral School of Clinical Medicine
Semmelweis University

Supervisor: Péter Sótonyi, M.D., Ph.D.

Official reviewers: László Benkő, MD, Ph.D.
Dávid Korda, MD, Ph.D.

Head of the Complex Examination Committee:
György Wéber, M.D., Ph.D.

Members of the Complex Examination Committee:
Ferenc Alföldy, M.D., Ph.D.
Eszter Végh, M.D., Ph.D.

Budapest
2022

Table of Contents:

List of abbreviations:

ΔTTP: Δ time to peak
2D3D: two dimensional to three dimensional
3D: three dimensional
4D: four dimensional
3D3D: three dimensional to three dimensional
BMI: body mass index
CBCT: cone beam computed tomography
CEUS: contrast-enhanced ultrasound
COPD: chronic obstructive pulmonary disease
CT: computed tomography
CTA: computed tomography angiography
d-CTA: dynamic time-resolved computed tomography angiography
d-MRA: dynamic magnetic resonance angiography
DLP: dose-length product
DSA: digital subtraction angiography
DUS: duplex ultrasound
ECG: electrocardiography
EVAR: endovascular aortic aneurysm repair
F/B-EVAR: fenestrated or branched endovascular aortic aneurysm repair
FEVAR: fenestrated endovascular aortic aneurysm repair
IMA: inferior mesenteric artery
IVUS: intravascular ultrasound
IQR: interquartile range between the first and third quartile
min-max: minimum – maximum
MRI: magnetic resonance imaging
ROI: region of interest
SD: standard deviation
t-CTA: triphasic computed tomography angiography
TAC: time attenuation curve

1. Introduction:

1.1. Endovascular aortic aneurysm repair

After the first successful infrarenal aortic aneurysm repair with a tube graft was described by Dubost, Allary and Oeconomos, there have been remarkable improvements in surgical techniques, graft materials, and patient care (1). Later on, open aortic aneurysm repair became the gold-standard management of infrarenal aortic aneurysms. The Cleveland Clinic group published their substantial experience showing good short- and long-term mortality results in 2002(2).

Then endovascular revolution happened.

Although open repair remains the preferred method in many cases, endovascular aortic aneurysm repair (EVAR) has become widespread over the last decade (3-5). In the United States between 2010 and 2016, over 80% of the intact infrarenal aortic aneurysms were treated with EVAR (3). In 2021 at Semmelweis University, EVAR was the preferred treatment option in around 66% of the cases for infrarenal aortic aneurysm management (6). A major reason of this is the minimal invasiveness of the procedure. In a recent study EVAR had a significantly lower 30-day mortality rate as compared to open repair, 1.1% vs. 4.6% in Hungary and 0.6% vs. 3.8% in the United States, respectively (3). Hidi and colleagues also reported a significantly lower in-hospital mortality after EVAR in both elective and ruptured infrarenal aortic aneurysm cases compared to open repair in Hungary (7). Another important factor in the success of EVAR is that nowadays the procedure is performed in a totally percutaneous fashion facilitating faster recovery and a less eventful postoperative period (8-10).

Despite the early survival advantage, incidence of graft-related complications (such as endoleak) and secondary intervention rates have been shown to be higher in patients who underwent EVAR than after open repair (11-13) (Fig. 1).

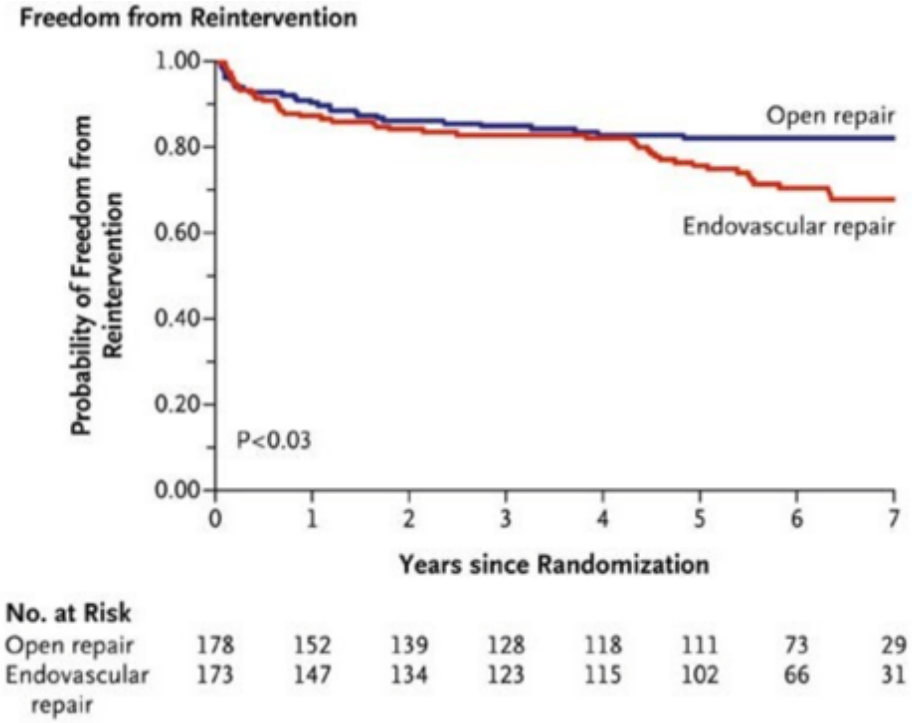

Figure 1. Freedom from reintervention after open and endovascular aortic repair, highlighting a significantly higher reintervention rate after 4 years in patients who were treated by endovascular means (11).

1.2. Imaging after endovascular aortic aneurysm repair - endoleaks

The increasing utilization of endovascular aortic aneurysm care in all aneurysm locations (juxtarenal, pararenal, thoracoabdominal, arch, and ascending aortic) (14, 15) requires developed imaging modalities to characterize aneurysm morphology and potential graft-related complications. The most common EVAR-related complications are endoleaks, which means persistent flow inside the aneurysm sac. These endoleaks are often considered as the Achilles heel of EVAR. Figure 2 displays the classification of endoleaks after fenestrated and branched EVAR (F/B-EVAR) (16).

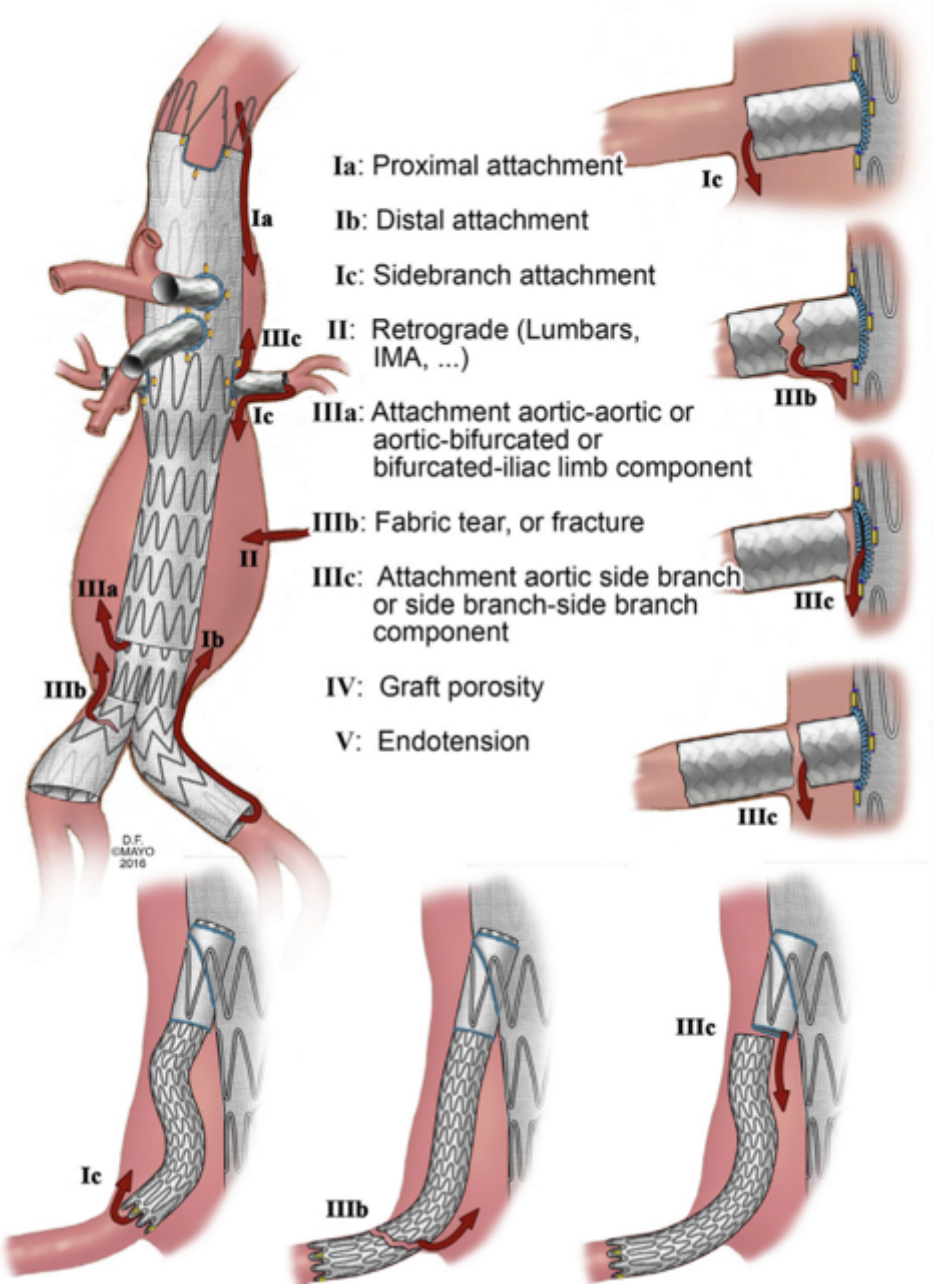

Figure 2. This image demonstrates the classification of endoleaks that can occur after fenestrated or branched endovascular aortic repair. Type II endoleak – retrograde flow in the aneurysm sac through lumbar or inferior mesenteric arteries – is the most common type (IMA-inferior mesenteric artery) (16).

Accurate diagnosis of endoleaks using adequate imaging surveillance and re-intervention contributes to better long-term outcomes of surgical treatment with aortic grafts, especially in the presence of aneurysm growth. Andersson and colleagues in their analysis

of 51 patients with rupture after EVAR reported type Ib and interconnection (type III) endoleaks to be a pre-cursor for long-term rupture in 61% of the cases and type Ia (proximal sealing error) in 39%, further highlighting the need for adequate surveillance to identify these pre-cursors (17).

Current guidelines recommend the use of computed tomography angiography (CTA) and duplex ultrasonography (DUS) as standard imaging modalities for follow-up after abdominal EVAR (4, 5). Figure 3 illustrates the currently recommended post-EVAR follow-up by the European Society for Vascular Surgery (5).

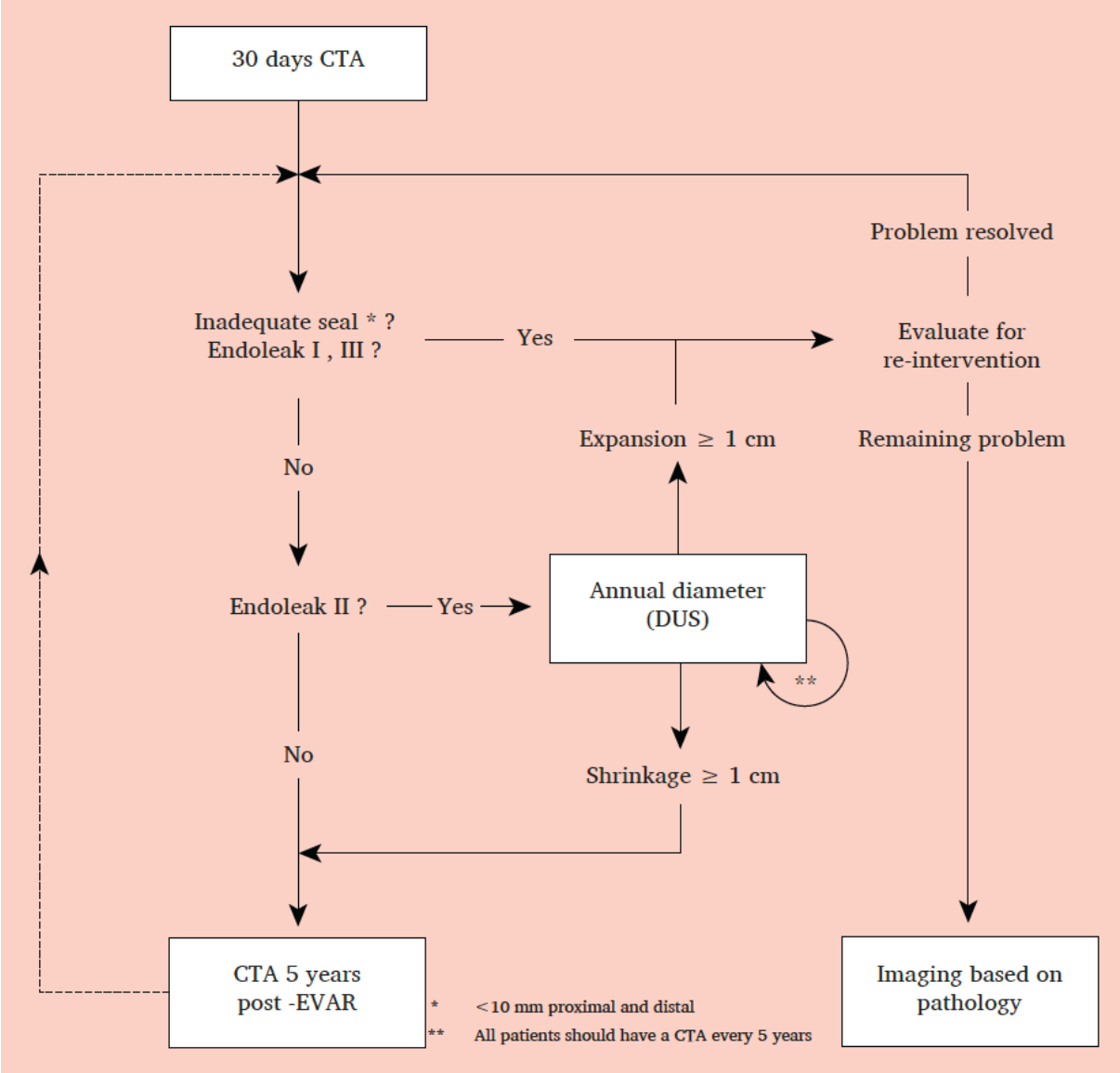

Figure 3. Imaging algorithm after EVAR as recommended by the European Society for Vascular Surgery. After the initial (30-day) CTA scan patients should have lifelong

surveillance with at least annual DUS and at least a repeated CTA scan after 5 years, or more frequent imaging with CTA if deemed necessary (5). DUS= duplex ultrasound, CTA= computed tomography angiography, EVAR= endovascular aortic aneurysm repair

The primary imaging modality after endograft implantation includes CTA using a triphasic (t-CTA) protocol (non-contrast, arterial, and delayed phase). This acquisition method allows image evaluation at three different timepoints: [1] before contrast injection, [2] after contrast injection but in less than a minute when the contrast material has a peak opacification inside the aorta (arterial phase), and another acquisition [3] when the peak opacification of the contrast material is in the venous system (venous phase). Lehmkuhl et al. reported a 73% endoleak detection rate using t-CTA imaging after EVAR, therefore, according to their study, around 30% of the endoleaks are missed by conventional t-CTA imaging (18). In their study a fairly new computed tomography (CT) imaging technique, called dynamic time-resolved CTA (d-CTA), showed a significantly better, 98% endoleak detection rate (18).

1.3. Dynamic imaging

Dynamic time-resolved imaging is an emerging subset of medical imaging techniques and has a high potential in understanding dynamic disease processes. This modality grants an ability to visualize flow velocity, direction, and volume and to functionally assess the region of interest (ROI).

Main modalities based on the different acquisitional background are ultrasound (DUS, echocardiography, intravascular ultrasound (IVUS), contrast-enhanced ultrasound (CEUS), dynamic magnetic resonance angiography (d-MRA) with or without four-dimensional (4D) flow analytic capability, digital subtraction angiography (DSA) (plus fluoroscopy), and dynamic time-resolved CTA.

Ultrasound being the most widespread modality has its well-known advantages as being a non-invasive, radiation free modality that is easy to access. In EVAR follow-up, DUS (alongside with CTA) is the most frequently performed modality (4, 5). Although it is limited in some ways (operator dependency, obese patients, graft infection, no fusion capability, difficult to standardize), using adjunctive microbubbles as contrast agents can further enhance diagnostic capabilities. IVUS warrants an additional benefit in

intraoperative imaging, particularly in aortic dissection (19). Figure 4 demonstrates a case when IVUS was used to detect and measure proximal landing zone before thoracic endograft deployment. This modality has been found to lead to improved long-term survival in patients with type B aortic dissection after thoracic EVAR (19).

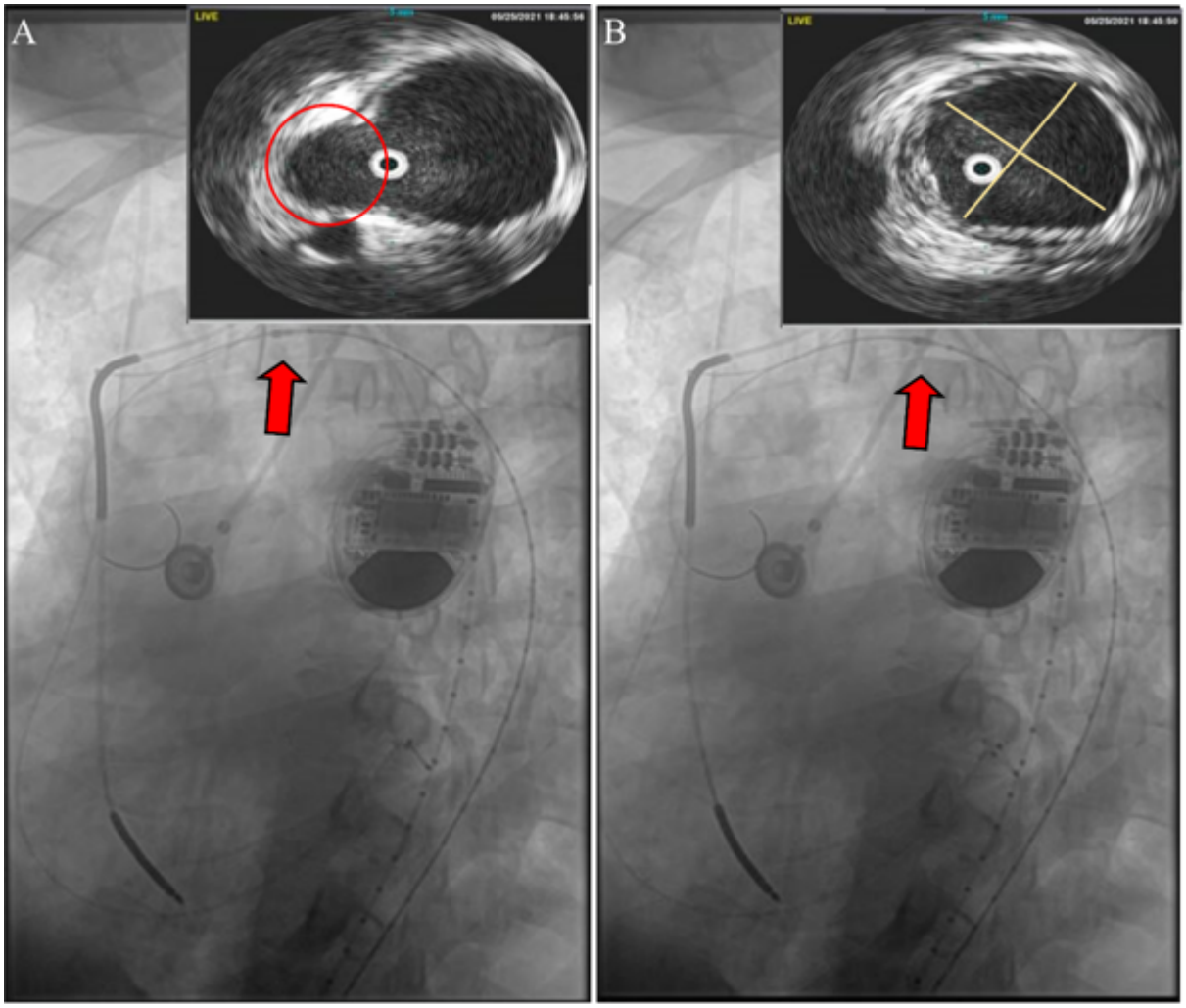

Figure 4. Intravascular ultrasound in use to detect proximal landing zone and measure aortic diameter (yellow lines in Fig.4B top panel) prior deployment of thoracic endograft. The transducer tip (red arrow) is positioned over-the-wire to detect the left subclavian artery orifice (red circle). (Case and figure from Houston Methodist Hospital).

D-MRA being a radiation-free and non-invasive imaging with 3D imaging capabilities, its better spatial and temporal resolution can provide insight into dynamic disease processes such as acute aortic dissection (20). Figure 5 highlights a case of a patient with aortic dissection imaged with d-MRA. In addition, novel, faster magnetic resonance

imaging (MRI) sequences can provide comprehensive physiological assessment of flow inside the aorta before and after treatment. For example, 4D flow imaging with multi-velocity encoding can provide flow patterns, peak velocity, pulse-wave velocity, and MRI-derived wall shear stress (21). With recent adoption of parallel imaging, novel image sampling and reconstruction techniques, acquisition time for 4D flow MRI imaging sequences have been reduced to less than 10 minutes. The d-MRA approach has similar limitations/challenges as conventional MRI. Image quality gets affected in the presence of metallic implants, stainless steel stents/coils, while image acquisition is limited in patients with claustrophobia or in patients who cannot tolerate longer image acquisition times.

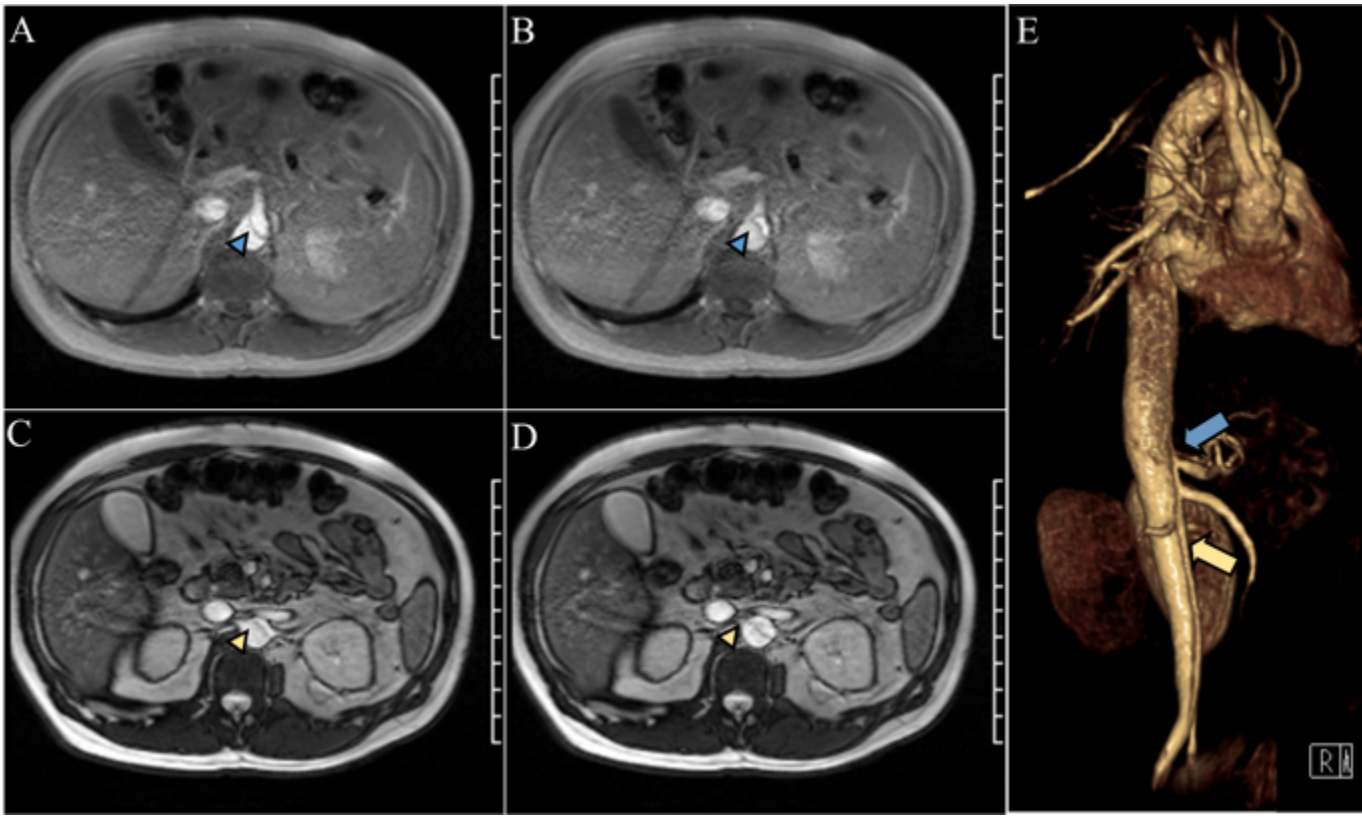

Figure 5. This figure illustrates a patient's steady-state free precession cine images at the level of the celiac trunk and renal arteries, as well as a 3D reconstructed image of the aorta. Figure 5A and 5B were taken at the same level with the same contrast opacification showing the dynamic movement of the dissection flap (blue arrowhead). This movement is visible at the level of the renal arteries (Fig. 5C and 5B), showing that both renal arteries arise from the true lumen and the mobile dissection flap causes a dynamic occlusion of

the right renal artery (yellow arrowhead). Dynamic MRA images can be used to generate 3D reconstructions as well, Fig. 5E shows such a reconstructed image of the same patient's aorta in diastole, yellow and blue arrows show the collapsed true lumen. (Case and figure from Houston Methodist Hospital).

1.4. Dynamic, time-resolved Computed Tomography Angiography

Dynamic, time-resolved computed tomography has been emerging rapidly with better scanner hardware and faster acquisition techniques. The application of dynamic, time-resolved CT angiography (d-CTA) imaging for diagnosing aortic endoleaks has been introduced with the evolution of third generation computed tomography (CT) scanners (18, 22-24). This imaging modality overcomes the limitation of having just two acquisition (time) points (early and delayed phase) after contrast injection. D-CTA enables three dimensional (3D) volumetric imaging across multiple time points along the contrast enhancement curve and has been shown to increase endoleak detection rate and better characterization of contrast enhancement mark of endoleaks (18, 22-24). The technique is available in latest CT scanners.

Aortic endoleak with sac enlargement can be hazardous and persistent type II endoleaks may even hide an occult type I or III endoleak (25). It has been reported that failed endoleak treatment may indicate a mis-diagnosed endoleak (25, 26) and make any further imaging studies challenging in the presence of coils/liquid embolic material due to limited image quality. This emphasizes the need for a reliable, non-invasive imaging technique in EVAR surveillance to identify the source of inflow into the aneurysm sac and to accurately characterize the type of the endoleak. The incidence of misdiagnosed/misclassified endoleak types using t-CTA has not been reported well in the literature.

Time-resolved, dynamic CT angiography involves multiple (~10-12) scan acquisitions after contrast injection enabling aneurysm sac imaging during the transit of contrast material across multiple time points (Figure 4) (27-31).

Having multiple scans along the contrast enhancement curve opens up a plethora of new aspects in characterizing endoleaks based on objective parameters, primarily on temporal Hounsfield unit change. A quantitative approach to endoleak differential diagnosis is a new concept which may aid in otherwise difficult cases.

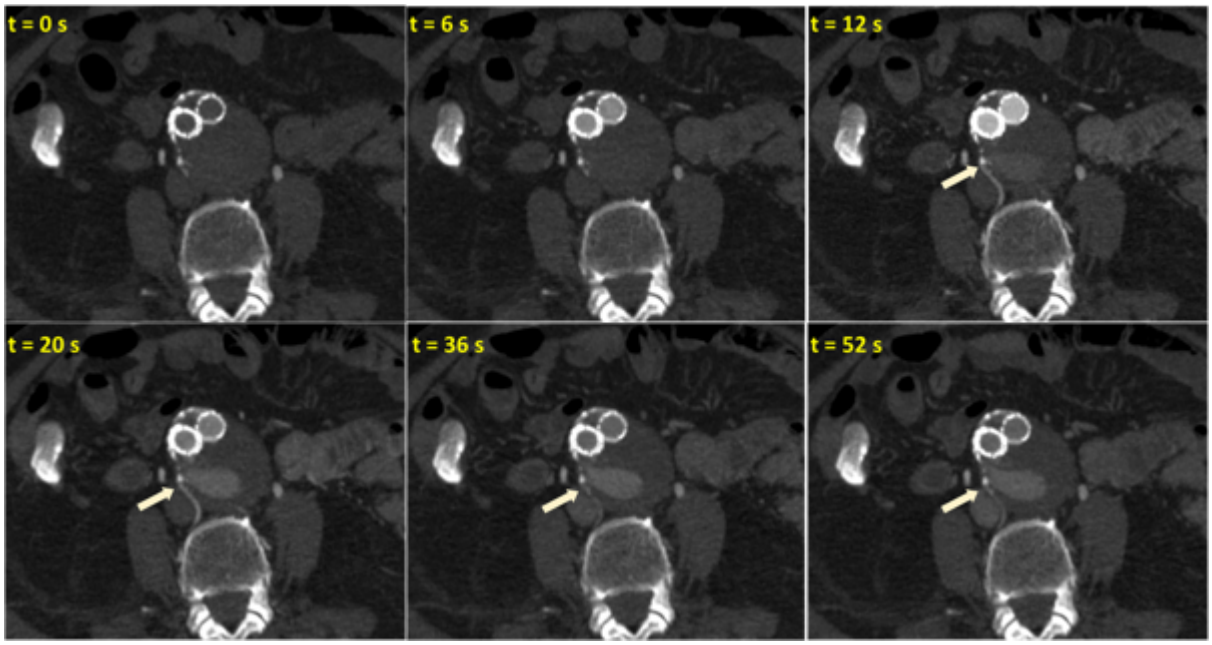

Figure 6. This figure illustrates an example of time-resolved axial CTA scans that were acquired in a patient having a type II endoleak from the L4 right lumbar artery. A delayed opacification of the L4 lumbar artery is highlighted with an arrow (29).

This time-resolved CT imaging technique can accurately identify endoleaks and has been shown to be the preferred method in patients with unclassified endoleak by standardized triphasic contrast enhanced CTA (29-31). Two dimensional (2D) DSA is the routinely used modality for confirming the type and source of endoleak. D-CTA imaging combines the benefits of time resolved contrast opacification with cross-sectional CT imaging, while being non-invasive and three dimensional. The endoleak embolization procedure often involves multiple diagnostic angiographies acquired at different C-arm angulations to identify the source of the endoleak. The target information from d-CTA can be utilized for intra-operative image fusion guidance during endoleak embolization (31).

1.5. Bridging diagnosis and therapy: image fusion

As preoperative 3D imaging has become fundamental in endovascular surgery, intraoperative imaging was limited to two dimensions using fluoroscopy and DSA for a longer period. The development of flat-panel detectors and cone beam CT (CBCT) capability had a remarkable impact on intraoperative imaging (32-34). The most promising clinical implication of these developments was image fusion (35). This technique enables the use of preoperative imaging not only for diagnostic purposes but for intraoperative planning and for procedural guidance as well. Correlating intraoperative 3D or 2D images to preoperative 3D imaging is based on anatomical landmarks or other components such as a previously implanted endograft (32). From a technical aspect, 2D3D and 3D3D co-registration exist. The difference is based on the intraoperative registration, utilizing two biplanar fluoroscopic (2D3D) views or a non-contrast CBCT (3D3D) (33,34). In order to align the two different modalities, the intraoperative workstation is used (Figure 7). The alignment can be done automatically but may need further finer alignments manually (30). Key landmarks on the preoperative image are marked. After accepting the image fusion, these landmarks are overlaid on top of real-time fluoroscopic images to guide the procedure (Fig. 8) (30). Of note, a selected dynamic CTA scan – the one with most information on the endoleak – can be used as part of image fusion which can reduce the otherwise long diagnostic phase of endoleak embolization (31).

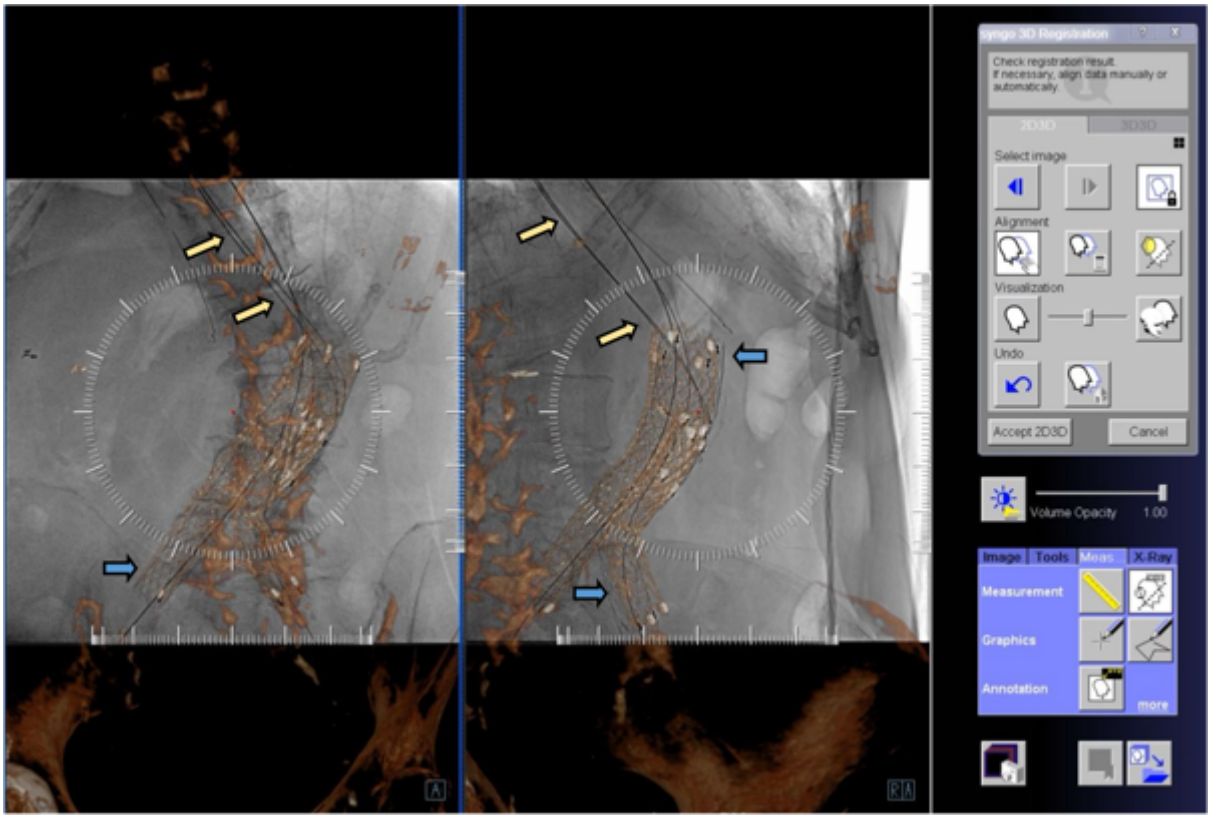

Figure 7. Display of the workstation for the alignment of the two 2D fluoroscopy images with the 3D d-CTA scan (2D-3D image fusion) prior to embolization. Yellow arrows depict the wires inside the aorta, blue arrows point to the endograft. The panel on the right is used to manually modify the automatic alignment: visualization of fluoroscopic and d-CTA imaging, different image selection, fine modification of alignment, accepting the alignment. Additional measurements and annotations can be made using the blue box on the right panel (30).

Figure 8. This figure demonstrates an embolization image of a patient who had a previous mis-aligned fenestrated-EVAR (FEVAR) and a bail-out chimney-EVAR with a type Ia gutter endoleak which was intervened using coil embolization after image fusion of the preoperative d-CTA scan. Yellow arrows show the coil as being deployed, endoleak cavity is marked with purple and one of the renal fenestrations is marked with a green circle. Horizontal blue and green lines are the orifices for the gutters, orange marker highlights the cranial end of the chimney graft (30).

2. Objectives:

2.1. 2.1. Study I - Comparison of standard and dynamic computed tomography angiography in endoleak diagnosis

After developing our dynamic CTA protocol for endoleak detection in patients who underwent EVAR, our first objective **(1)** was to explore if d-CTA has better endoleak type diagnosing capability compared to t-CTA when using DSA as baseline reference.

In addition to determining endoleak type, our second aim **(2)** was to compare the radiation exposure during image acquisition with the two CT modalities.

Our third objective **(3)** was to match d-CTA, t-CTA, and DSA in detecting the number of inflow vessels in patients diagnosed with type II endoleak.

2.2. 2.2. Study II - Quantitative approach to characterize endoleak types

Time-resolved CTA acquisition opens up a plethora of new aspects to characterize endoleaks based on objective/quantitative parameters.

After developing our quantitative image analysis protocol, our fourth objective **(4)** was to demonstrate the feasibility of a quantitative parameter aiding the differential diagnosis of endoleak types.

In this study, similar to our third objective, **(5)** we matched d-CTA and DSA in detecting the number of inflow vessels in patients diagnosed with type II endoleak.

3. Methods:

Study protocols were approved by the Institutional Review Board of Houston Methodist Hospital Research Institute (PRO00026403). Studies were carried out according to the principles of the Declaration of Helsinki.

3.1. Image acquisition

The acquisition incorporated fast spiral scans in a limited scan range from the celiac trunk to the internal iliac arteries. First a topogram scan was performed to orient scan position and estimate the region of interest. Then ~14-20 ml iodinated contrast material (320 mg/ml Visipaque, GE Healthcare, Chicago, Illinois, USA) at 3.5-4 ml/sec flow rate was injected, followed by a saline bolus as part of "test bolus" to measure dye arrival in the aorta proximal to the graft. Then multiple scans (10-12) were distributed along the contrast enhancement curve and acquired after another (70-90 ml) contrast injection followed by ~80ml saline injection from peripheral vein access. The number of scans and their distribution were customized based on previous scans, suspected endoleak, and timing of the initial iodinated contrast injection. The average scan range was 23-33 cm to achieve adequate coverage. To enhance the scan range, short rotation time and bidirectional table movement ("shuttle mode") were needed (30). Tube voltage was optimized for each patient to mitigate radiation exposure. The scans were performed using a dual-source CT scanner (Somatom Force CT, Siemens-Healthineers, Erlangen, Germany). Table 1 demonstrates the customized dynamic CTA acquisition protocol to detect endoleak after EVAR (29).

Table 1. Parameters of the image acquisition protocol (29).

Protocol	DynMulti4D
Total number of volumes	10-12 scans - 2-4 scans @ every 1.5 seconds - 4 scans @ every 3 seconds - 2-4 scans @ every 4.5 seconds
Tube voltage	70-100 kV
Tube current	150 mAs
Rotation time	0.25 sec
Pitch	1
Scan duration	39 seconds
Slice thickness	0.7 – 1 mm
Contrast material volume	70-90 ml
Flow rate	3.5 – 4 ml/sec
Saline flush	90-100 ml
Scan range (z-axis)	23-33 cm

3.2. Image analysis

The acquired images were then analyzed using syngo.via (Syngo.via, VB30, Siemens Healthineers, Erlangen, Germany) and a dedicated dynamic CTA workflow. This workflow can eliminate misalignments that happened during patient movement and breathing using a motion correction algorithm. After correction, qualitative analyses were performed in multiplanar and volume-rendered reconstructions in both still and cine mode (30). Endoleak assessment was performed on a systematic approach ruling out endoleaks from (1) proximal and distal sealing zones, (2) graft related complications, and (3) aortic side-branches.

3.3. Study I - Comparison of standard and dynamic computed tomography angiography in endoleak diagnosis

In this retrospective review, a total of 52 patients underwent d-CTA image acquisition after EVAR between 2019 March and 2021 July at the Cardiovascular Surgery Department of Houston Methodist Hospital. Amongst them, we selected patients with available triphasic and dynamic CTA images who had DSA acquisition in order to visualize potential endoleaks after EVAR within a three-month period and no interim interventions (31).

Triphasic CTA acquisitions were performed at Houston Methodist Hospital using Somatom Force CT scanner (Siemens-Healthineers, Erlangen, Germany). Difference compared to d-CTA scan was that all of the scans were acquired at 120 kV covering the total abdomen and pelvis.
DSA images were acquired at Houston Methodist Hospital using Artis Pheno or Artis Zee fixed C-arm angiography systems (Siemens-Healthineers, Erlangen, Germany) after EVAR implantation (not as completion angiography).

3.3.1. Qualitative image review

Triphasic and dynamic CTA images were reviewed with syngo.via (Syngo.via, VB30, Siemens Healthineers, Erlangen, Germany). DSA images were analyzed in Horos dicom file viewer (Horos Project, New York, USA). Images were de-identified and put in a randomized order. For the expert review of CTA images, two senior vascular imaging specialists and for the DSA image review two senior vascular surgeons were involved in the analysis of the images. Presence of endoleak, type of endoleak, and, if deemed necessary, inflow/target vessels contributing to type II endoleak were also recorded. Discrepancy between reviewers was solved by consensus.

3.4. Study II - Quantitative approach to characterize endoleak types

In this retrospective review patients undergone d-CTA and DSA image acquisition after EVAR between 2019 March and 2021 January at the Cardiovascular Surgery Department of Houston Methodist Hospital were selected (24).

DSA images were acquired at Houston Methodist Hospital using Artis Pheno or Artis Zee fixed C-arm angiography systems (Siemens-Healthineers, Erlangen, Germany) after EVAR implantation. The DSA images were acquired using flush or selective catheters. No completion angiography after EVAR was selected for review.

3.4.1. Qualitative analysis

Dynamic CTA images were reviewed with syngo.via (Syngo.via, VB30, Siemens Healthineers, Erlangen, Germany). DSA images were analyzed in Horos dicom file viewer (Horos Project, New York, USA). Images were de-identified and put in a randomized order. For the expert review of CTA images two senior vascular imaging specialists and for the DSA image review two senior vascular surgeons were involved in the analysis of the images. Presence of endoleak, type of endoleak, and, if deemed necessary, inflow/target vessels contributing to type II endoleak were also recorded. Discrepancy between reviewers were solved by consensus.

3.4.2. Quantitative analysis

Quantitative endoleak analysis being a new concept- to aid endoleak differential diagnosis based on temporal Hounsfield unit change, we selected two different ROIs for analysis: (1, ROI_{aorta}) in the aorta at the level of the proximal graft and (2, $ROI_{endoleak}$) one inside the aneurysm sac where contrast enhancement was detected. Then the software generated the corresponding time attenuation curves (TAC) for each ROI. TAC has multiple quantitative parameters that can be used for analysis, we selected the relative time difference between ROI_{aorta} and $ROI_{endoleak}$ in reaching peak enhancement. Figure 9 demonstrates the quantitative image analysis of a time attenuation curve. Our practice focused on endoleak specific Δtime to peak values (ΔTTP) to highlight the difference in reaching peak enhancement between aorta and endoleak (30). In type II endoleak cases suspected target vessels can be selected for further analysis which can determine in- and outflow vessels contributing to the endoleak and aid future embolization. Quantitative analysis was performed using the dynamic CTA workflow of syngo.via (Syngo.via, VB30, Siemens Healthineers, Erlangen, Germany).

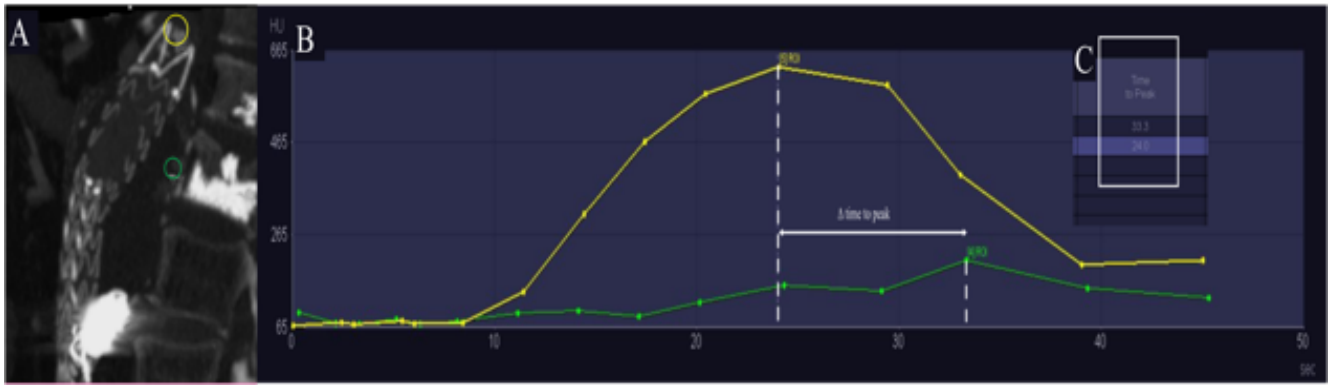

Figure 9. Example of a time attenuation curve analysis in a patient having a type II endoleak from a lumbar artery as inflow. (Fig. 9A) The selected region of interest (yellow above the stent-graft (ROI_{aorta}), green inside the aneurysm sac where endoleak is visualized ($ROI_{endoleak}$)). Fig. 9B demonstrates the generated time-attenuation curves for the selected ROIs in Fig. 9A. Time difference between aortic and endoleak curves in reaching peak Hounsfield unit is recorded (Δ time to peak value - marked with white) (ROI=region of interest) (The figure was created for the thesis).

3.5. Statistical analysis

Statistical analyses were performed using SPSS v.27 (SPSS Inc, Chicago, Il, USA). Continuous variables are presented as median (interquartile range) or mean (± standard deviation), categorical variables are presented as frequency and proportion. Continuous, not normally distributed, dependent variables were analyzed by Wilcoxon-signed rank and Friedman's test. Continuous, not normally distributed independent variables were analyzed by Wilcoxon rank sum and Kruskal-Wallis test. P-value of 0.05 or less indicated a significant difference.

4. Results:

4.1. 4.1. Study I - Comparison of standard and dynamic computed tomography angiography in endoleak diagnosis

4.1.1. Patient selection

From the 52 patients who underwent d-CTA acquisition in the study period, 19 met the criteria for selection. In this study population 15 out of 19 patients had conventional EVAR, 3 had FEVAR, and 1 had chimney EVAR. Target vessels for the complex EVARs bridged with covered stents were renal arteries only (n=8).

Mean (±Standard Deviation [SD]) age, serum creatinine, and body-mass index (BMI) before image acquisition were 78.8 (±6.8) years, 97.3 (±26.5) μmol/L, and 25.8 (±5.8) m^2/kg, respectively. Table 2 highlights the baseline characteristics of the cohort.

Table 2. Baseline patient characteristics, *=BMI indicates body-mass index, **= 1 patient was on regular dialysis, so her creatinine value was excluded, if left included (1.34±1.04), ***COPD chronic obstructive pulmonary disease.

Patient characteristics (n=19)	
Age (mean±SD)	78.9 (±6.8) years
Sex (male, %)	16 (84.2%)
BMI* (kg/m^2, mean±SD)	25.8 (±5.8)
Creatinine (mg/dl, mean±SD)	1.10(±0.3)**
Diabetes mellitus (n, %)	3 (20.0%)
Previous stroke	4 (21.1%)
Coronary artery disease	10 (52.6%)
Smoking	9 (47.4%)
COPD***	4 (21.1%)
Hypertension	18 (94.7%)
Hyperlipidemia	14 (73.7%)

4.1.2. Qualitative analysis of triphasic and dynamic computed tomography angiography

D-CTA findings matched with DSA findings in 19 out of 19 cases (100%), while t-CTA findings matched 14/19 (73.7%). Figure 10 demonstrates the findings of the qualitative image review. Out of five patients who had a mismatch between t-CTA and DSA, two were discordant, and three were inconclusive for the type of endoleak (31).

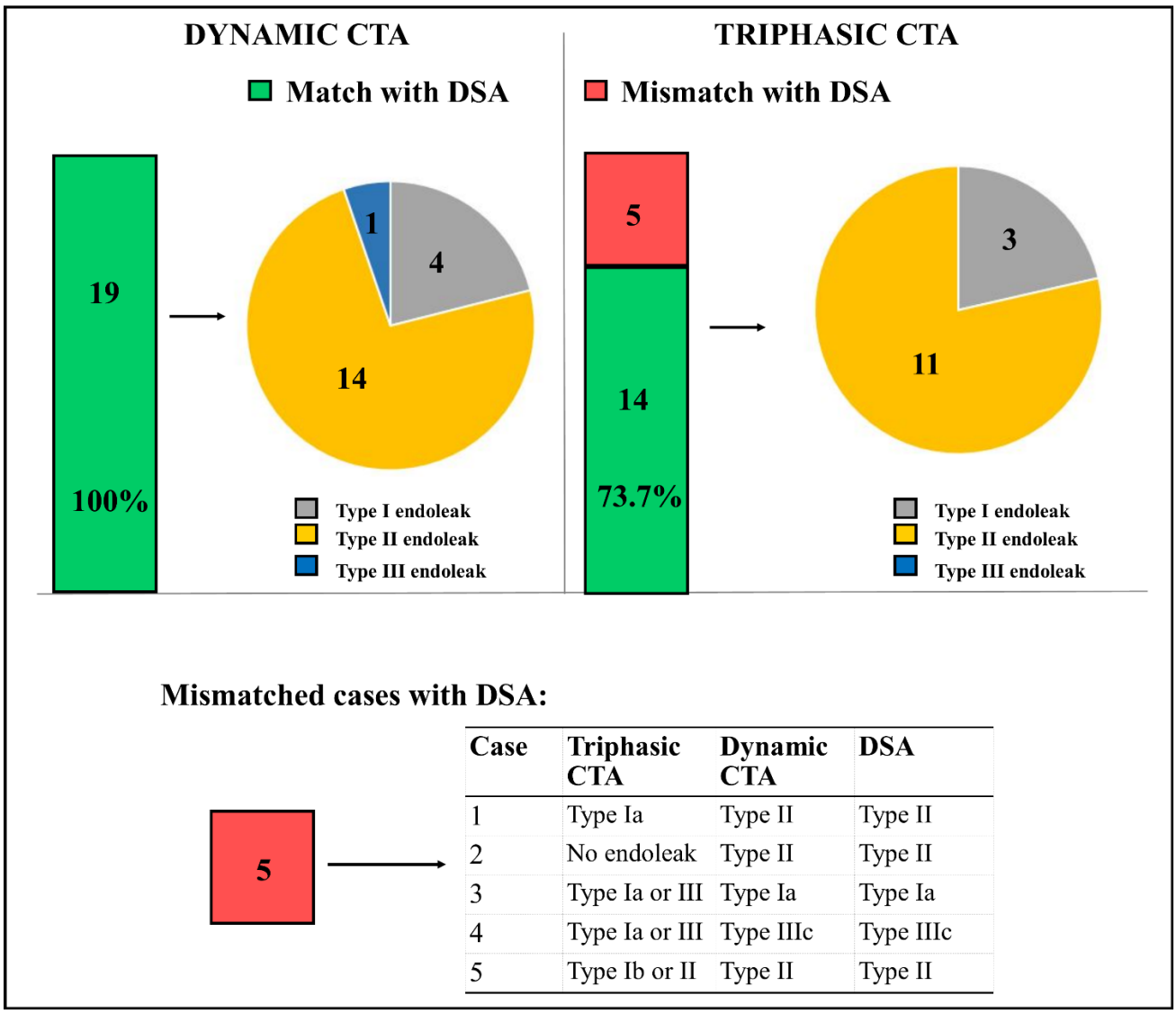

Case	Triphasic CTA	Dynamic CTA	DSA
1	Type Ia	Type II	Type II
2	No endoleak	Type II	Type II
3	Type Ia or III	Type Ia	Type Ia
4	Type Ia or III	Type IIIc	Type IIIc
5	Type Ib or II	Type II	Type II

Figure 10. Findings of the qualitative image review. Dynamic CTA was compared to triphasic CTA, and DSA was used as reference standard (31).

Figure 11 illustrates a patient in whom t-CTA did not identify an endoleak, while d-CTA and DSA imaging demonstrated a type II endoleak from an inferior mesenteric artery (31). T-CTA imaging was inconclusive in three cases: [1] post-FEVAR t-CTA imaging was read as possible type Ia or type III endoleak, while d-CTA and DSA confirmed a type IIIc endoleak from the left renal fenestration (Figure 12) (31), [2] t-CTA imaging showed possible I or III endoleak, while d-CTA and DSA confirmed type Ia endoleak, [3] t-CTA imaging showed possible Ib or II endoleak, while d-CTA and DSA confirmed a type II endoleak from L5 lumbar artery.

In 11 patients, where type II endoleak was confirmed, the number of target arteries identified by d-CTA, t-CTA, and DSA were 23, 17, and 16 respectively (p=0.009), and d-CTA identified more target vessels than t-CTA (p=0.034).

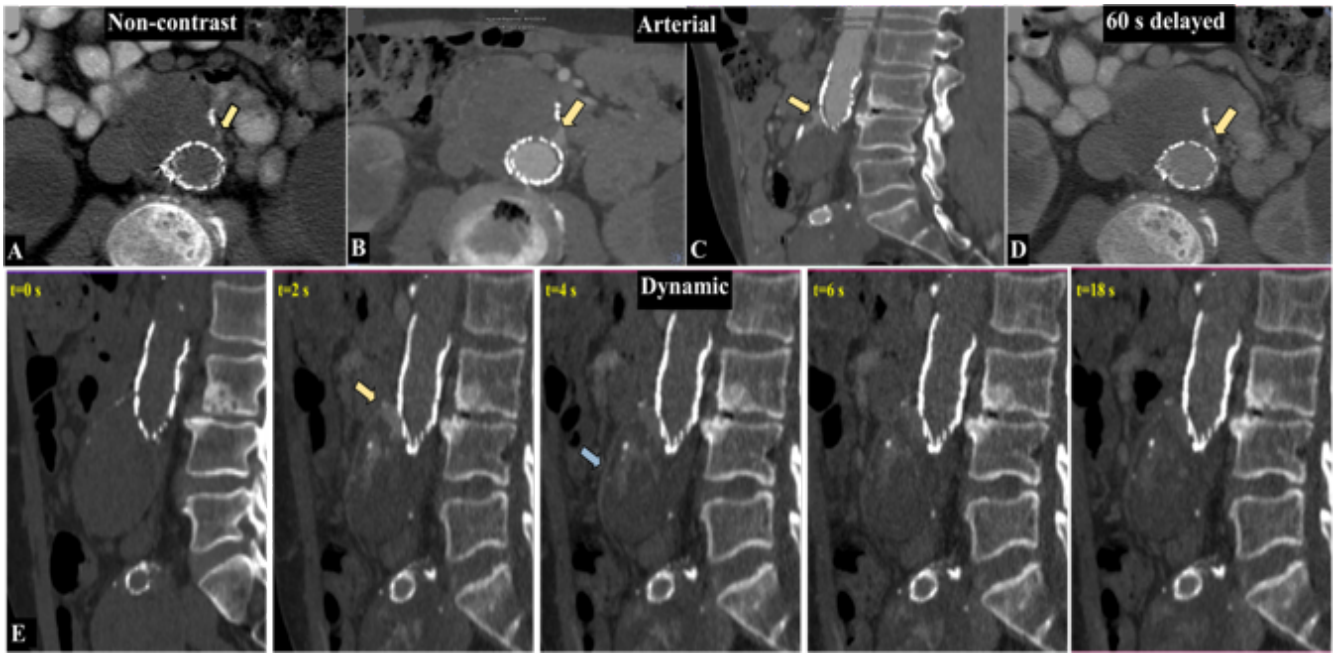

Figure 11. This image demonstrates triphasic (Fig. 11A-11D) and dynamic CTAs (Fig. 11E). After the qualitative review discordant findings were reported. D-CTA images matched with DSA findings diagnosing a type II endoleak from an inferior mesenteric artery (yellow arrow) (31).

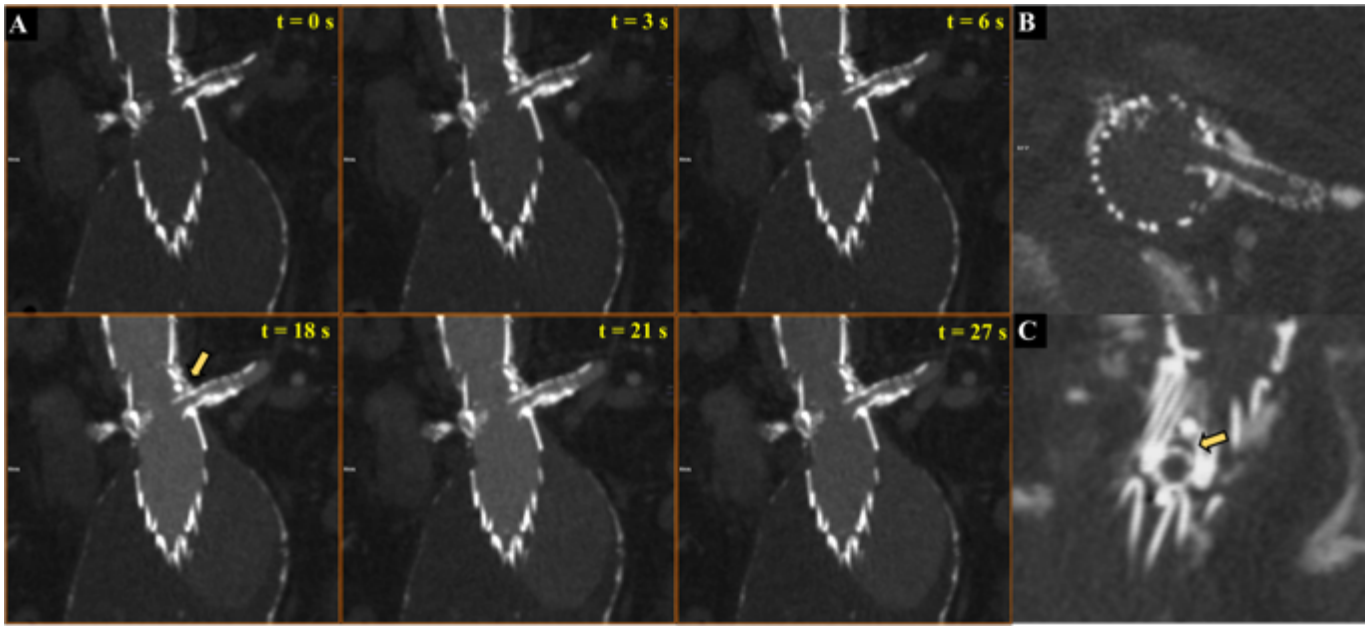

Figure 12. This image depicts a type IIIc endoleak after a FEVAR. The source of the endoleak was a size mismatch between the left renal fenestration and the diameter of the left renal covered stent. Yellow arrow on Fig. 12C highlights the gap and the contrast enhancement creating a type IIIc endoleak at the 18th second of the acquisition (31).

4.1.3. Comparison of radiation exposure

The mean (±SD) dose-length product (DLP) for d-CTA and t-CTA were 1445 (±550) and 1612 (±530) mGy*cm, respectively (p=0.255) (Figure 13) (31). Although the DLP values showed no significant difference, it is important to emphasize the differences in acquisition protocols. Dynamic scans were acquired at 80 (interquartile range 70-97.5) kV tube voltage with the scan field of view covering the implanted stent graft only (23-33 cm), while triphasic scans were acquired at 120 kV covering the entire abdomen from diaphragm to pelvis.

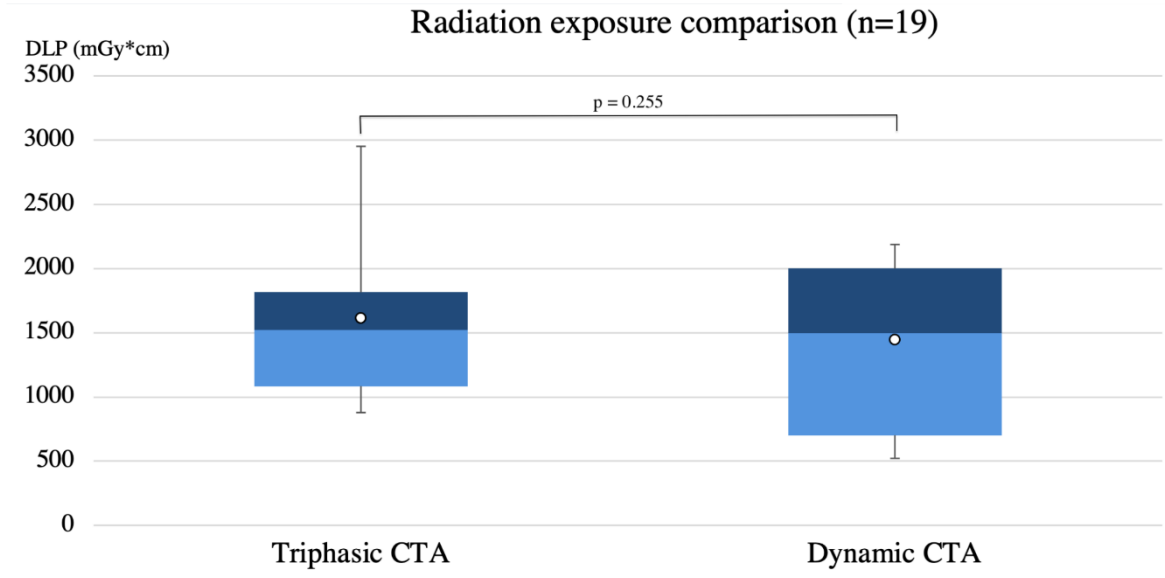

Dose-length product (mean± SD)	1612.3±530.3	1445.1±550.5
Tube voltage (kV, median, IQR)	120	80 (70-97.5)
Scan range	Abdomen, pelvis	23-33 cm

Figure 13. Comparison of radiation exposure between t-CTA and d-CTA (IQR=interquartile range between the first and third quartile) (31).

4.2. 4.2. Study II - Quantitative approach to characterize endoleaks

4.2.1. Study cohort and baseline demographics

From the 24 patients 3 underwent chimney-EVAR, 3 had FEVAR, and 18 underwent conventional EVAR. Target vessels for the complex EVARs bridged with covered stents were renal arteries only (n=12).

Mean(±SD) age, serum creatinine before d-CTA imaging, and BMI were 78(±7.11) years, 99.9 (±31.0) μmol/L mg/dl, and 26.37 (±5.31) m^2/kg, respectively (Table 3). The mean (±SD) dose-length product for d-CTA was 1038 (±533) mGy*cm for a total of 12 scans. Total iodinated contrast volume used for d-CTA was 77.1 (± 5.4) ml.

Table 3. Patient demographics *=BMI indicates body-mass index, COPD chronic obstructive pulmonary disease

Characteristic	Overall
Age (y, mean±SD)	78 (±7.11)
Sex (male, %)	16 (66.7%)
BMI* (kg/ m^2, mean±SD)	26.37 (±5.31)
Creatinine (mg/dl, mean±SD)	1.13(±0.35)
Diabetes mellitus (n, %)	4 (16.7%)
Previous stroke	8 (33.3%)
Coronary artery disease	9 (37.5%)
Smoking	10 (41.7%)
COPD*	6 (25%)
Hypertension	22 (91.7%)
Hyperlipidemia	18 (75%)
Previous coil embolization for endoleak	8 (33.3%)

4.2.2. Qualitative image review

In 23/24 patients (95.8%), d-CTA findings correlated with DSA findings for endoleak type. In one patient, d-CTA demonstrated type III endoleak, whereas no evident endoleak was visible on DSA imaging (Table 4) (24). This patient underwent an Ovation® (Endologix Inc., Irwine, USA) graft implantation and d-CTA imaging demonstrated the defect in one of the polymer sealing rings leading to type III endoleak (Figure 14), which was later relined (24). In the 16 cases of types II endoleak, d-CTA identified significantly more vessels (lumbar arteries) contributing to the endoleak as compared to DSA (33 vs 21, p=0.010).

Figure 14. The discrepant finding between d-CTA and DSA in a patient after infrarenal Ovation® (Endologix Inc., Irwine, USA) graft repair. Red arrowheads show the graft's polymer sealing ring and on Fig.14A yellow arrowhead highlights the defect of the ring, the asterisk marks the subsequent type III endoleak that was not visible on standard DSA imaging (24).

Table 4 summarizes findings on endoleak types and inflow vessels based on qualitative image review of d-CTA and DSA imaging. In type II endoleak cases, d-CTA identified more feeding vessels than DSA imaging (33 vs 21 vessels, p=0.010) (24).

Endoleak type	Diagnostic Imaging Modality (n=24)		Inflow vessels of endoleak	
	Dynamic CTA	DSA	Dynamic CTA	DSA
I	4	4	Ia seal zone (1), Ia gutter endoleak (3)	Ia (4)
II	16	16	**Lumbar a. (29)** RRA (1) IMA (3)	Lumbar a. (17) RRA (1) IMA (3)
III	**3**	2	Component separation, graft defect, **polymer sealing ring defect**	Component separation, graft defect
No endoleak	1	**2**		

4.2.3. Quantitative endoleak analysis

Quantitative time-attenuation curve analysis was performed in 23/24 patients, while one patient in our study did not show any contrast enhancement in the aneurysm sac by d-CTA imaging. Amongst 23 patients, Δ TTP values (median, IQR) between ROI_{aorta} and $ROI_{endoleak}$ was 1.64 (0.26-3.17) seconds for type I (n=4), 10.45 (8-12) seconds for type II (n=16), and 5 (4.78-6.05) seconds for type III endoleak (n=3), respectively (p=0.002) (Figure 15). ΔTTP was significantly shorter for type I (p=0.003) and III (p=0.043) endoleaks as compared to type II endoleak.

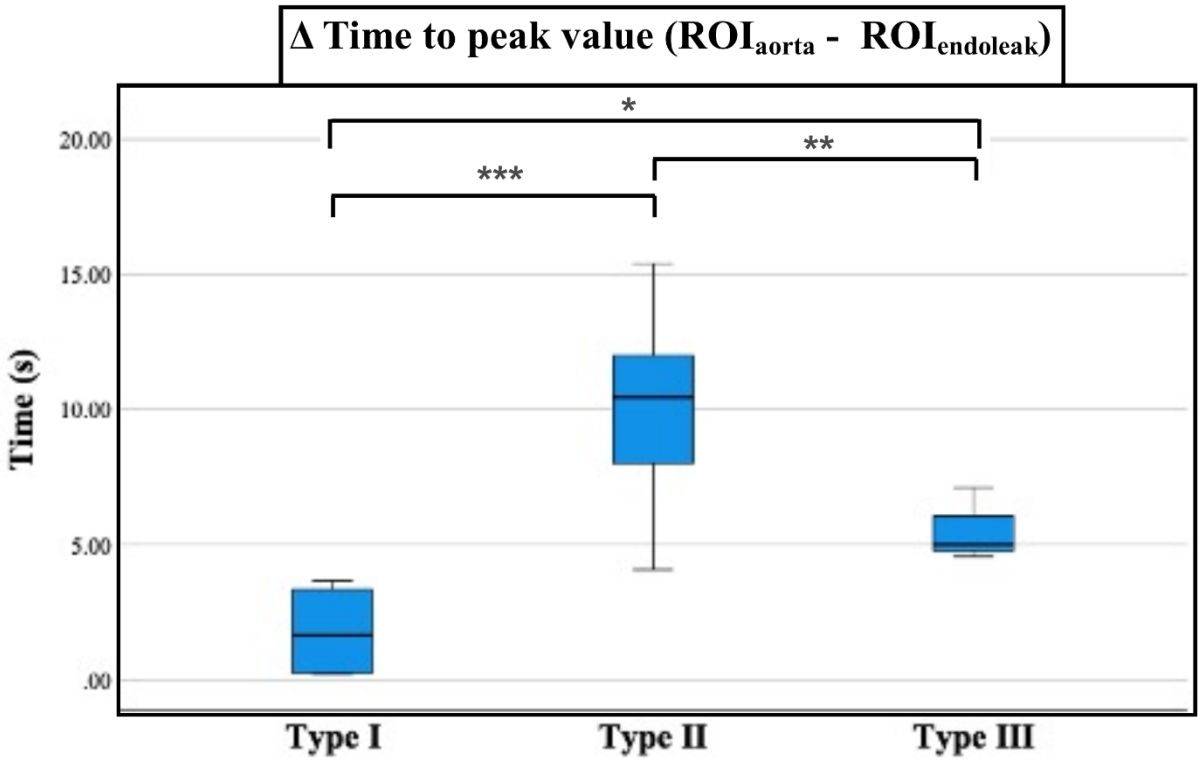

	Type I (n=4)	Type II (n=16)	Type III (n=3)
Median	1.64 s	10.45 s	5 s
Q1	0.26 s	8 s	4.78 s
Q3	3.17 s	12 s	6.05 s
Minimum	0.20 s	4.07 s	4.55 s
Maximum	3.66 s	15.40 s	7.10 s

Figure 15. Box and whiskers plot summarizing the Δ time to peak (TTP) values between ROI_{aorta} and $ROI_{endoleak}$ in 23 patients, grouped by endoleak type (*=p-value for Kruskal-Wallis test:0.002, **=p-value for Wilcoxon rank sum test comparing type I and II endoleaks: 0.003, ***=p-value for Wilcoxon rank sum test comparing type II and III endoleaks: 0.043) (The figure was created for the thesis).

5. Discussion:

In this thesis we describe our approach with dynamic, time-resolved CTA imaging using both qualitative and quantitative methods to better characterize endoleaks after endovascular aortic repair. Based on our results, this approach was more accurate in diagnosing endoleaks compared to current standard of care triphasic CTA at a reasonable level of radiation exposure. D-CTA imaging also made the identification of more target vessels contributing to endoleaks, which can be targeted upon later embolization.

This time-resolved acquisition method not only demonstrated better visualization of flow patterns but can further aid endoleak characterization utilizing objective parameters such as Δ time to peak value.

In contrast with type I and III endoleaks, the management of type II endoleaks – especially in the absence of aneurysm growth- has been a matter of debate for long time (35-37). An important reason to be taken into consideration is that type II endoleak treatment is associated with poor clinical outcome and with the majority of patients presenting with recurrent/persistent endoleaks at follow-up visits (38). Moreover, systematic reviews highlighted a less than 2% rupture rate after EVAR secondary to type II endoleaks (39,40). Failure in treatment of type II endoleaks/ persistent endoleaks on repeated imaging and the presence of aneurysm growth can lead to delayed rupture attributed not only to incomplete embolization but to misdiagnosed endoleaks –occult type I or III- as well (25, 39, 41). Although a recent study focusing on clinical outcomes in patients treated with expanding aneurysm highlighted high technical success in type II endoleak embolization, high recurrence and multiple re-interventions were also needed to stabilize sac growth (42). Notably, the authors stated that one in five patients treated with type II endoleak had concomitant type I endoleak from losing proximal or distal sealing zone that was not initially recognized (42). These studies underline the fact that thorough assessment is needed prior to performing endoleak treatment after EVAR and highlight the need for a robust surveillance method in the presence of aneurysm growth. This is even more relevant with the expansion of EVAR to more complex aneurysm management.

Here, we discuss our experience using dynamic CT angiography in EVAR follow-up to detect endoleaks and to emphasize its value in targeted embolization. Studies using dynamic imaging for aortic endoleak detection has been published previously (18,22-24). Lehmkuhl and colleagues highlighted the advantage of using multiple scans over standard triphasic CTA by analyzing contrast enhancement patterns inside the aneurysm sac (18). This publication reported that d-CTA scans acquired 27 seconds after the peak enhancement had significantly higher endoleak detection rate as compared to arterial and delayed phase imaging (98% vs 73%) (18). The rationale behind this difference is that many endoleaks show contrast enhancement in the time interval between the arterial and the delayed phase (acquired around 60 to 100 seconds) scans. Hou et al. in their prospective trial demonstrated a 100% accuracy in endoleak diagnosis using d-CTA in cases that were difficult to characterize with standard t-CTA (24). In this pilot-study an additional overall radiation reduction was also achieved when intervention for endoleaks was encountered (23). An additional interesting observation of ours was imaging patients with retroaortic left renal vein and previous endovascular aortic repair (43), which unique anatomical variation on dynamic imaging can mimic type I endoleak based on the contrast enhancement marks in the vein adjacent to the proximal landing zone of the previous EVAR.

The routine application of d-CTA in clinical practice has not yet come. Many argue that having a greater number of scans will result in higher radiation exposure, thus leading to a significant cost when using this advanced imaging modality. However, according to our findings, optimized CT scans with lower kV and smaller longitudinal scan range resulted in a mean DLP value of 1445 for d-CTA acquisition which was comparable/similar to the radiation burden of standard triphasic scans. It is important to emphasize that triphasic CTA scans were acquired at higher kV with larger longitudinal coverage not optimized for each patient and for endograft coverage only. In the literature various values have been reported with different acquisition protocols (18, 19, 24, 38,39). The reported mean DLP values range from 875 to 1064 mGy*cm with only Apfaltrer and colleagues reporting slightly higher radiation when compared to t-CTA (1064 vs 878 mGy*cm) (18, 22, 23, 44,45). Regarding d-CTA acquisition-related radiation exposure it is important to accentuate that there is an inevitable learning curve on how to optimize scans (timing of contrast, scan distribution, optimal kV setting) (30). Based on

experience, patient BMI was an important factor when kV setting was defined (30). Hopefully in the future, with model-based iterative reconstruction this can be further optimized and d-CTA scans can be performed to shorten this learning curve.

Obtaining multiple scans along the contrast enhancement curve not only helps qualitative analysis but grants a new quantitative approach to endoleak analysis, which is based on objective parameters (temporal Hounsfield unit change). Apfaltrer and colleagues enhanced qualitative assessment with color-coded blood perfusion map of the aneurysm sac based on TAC curves (45). This approach yielded a better endoleak diagnosing capability with d-CTA. Similar perfusion imaging was used in a pilot study to categorize type II endoleaks into high and low-risk groups for aneurysm growth after EVAR with promising results (46). In our study Δ time to peak values from the TAC were significantly different in type I and type II endoleaks this may aid differential diagnosis which can be difficult to characterize on standard imaging (Fig. 9, 10) (24). Using these objective parameters or other potential characteristics (e.g., slope of the enhancement patterns in the ROI) aid endoleak characterization and may serve as a basis for future automated analyses and bring more objectivity and reproducibility into endoleak diagnosis.

High accuracy in endoleak diagnosis will not mean unambiguously good outcome and a low rate of persistent/recurrent endoleak in all cases. According to recent studies, patients with larger aneurysms were found to have higher rates of reintervention and persistent type II endoleaks (47, 48). This may be associated with the number of inflow vessels contributing to the endoleak. We found that an additional benefit of using d-CTA imaging in patients with suspected type II endoleaks and aneurysm growth was in identifying more target vessels contributing to the endoleak as compared to conventional t-CTA or DSA imaging. In our theory, these potentially missed target vessels on conventional imaging can result in persisting endoleaks. Furthermore, identifying the exact pathomechanism of type II endoleaks (i.e., in- and outflow vessels) can further mitigate radiation exposure and contrast volume consumption during treatment (24).

Another aspect of utilizing d-CTA imaging in endoleak surveillance is the capability to guide endoleak embolization. Our detailed approach of implementing d-CTA into endoleak treatment via fusion guidance was described earlier (30,31). There are several publications emphasizing the benefits of using image fusion guidance in endovascular

procedures, such as reduction in radiation exposure, contrast volume consumption, and procedural time (49-53). In one of our studies, we aimed to highlight the advantage of image-fusion techniques combined with the high accuracy of d-CTA by demonstrating a reduction in radiation exposure in the diagnostic phase of the intervention (31). A shorter procedural time was reported by others utilizing image-fusion in endoleak treatment as compared to cases when fusion was not used (53,54). When d-CTA-based endoleak interventions were compared to t-CTA-based treatment, Hou et al also reported a reduction in the number of diagnostic angiographies (1 vs. 6) and overall radiation exposure of patients undergone d-CTA (22). Given the limited sample size, we did not pursue a comparison of 2D3D and three dimensional to 3D3D fusion techniques, but it is apparent to underline that the 3D3D technique has an inevitably higher radiation burden as opposed to 2D3D based on the fact that a cone beam CT is acquired in the former and only two perpendicular fluoroscopic images in the latter.

Throughout this thesis the main focus was on computed tomography imaging, however, other modalities offer promising solutions to detect endoleaks after EVAR such as CEUS. Besides evident differences between CT and DUS in terms of radiation, nephrotoxic contrast agent use and operator dependency DUS are widely adopted in EVAR surveillance. CEUS uses microbubbles as contrast material - similar in size to red blood cells - that stay in the circulation and do not infiltrate into extravascular tissue. Several studies focused on the use of CEUS in EVAR surveillance reporting high sensitivity (55, 56). When compared to conventional CTA, CEUS showed similar sensitivity in an earlier study (57) and even better in a more recent systematic review, although CEUS was inferior to evaluate diameter change over time (58). An even more advanced three-dimensional CEUS was compared to conventional CTA by Lowe et al. This newer technology outlined remarkable specificity (100%) and sensitivity (96%) in endoleak diagnosis, superior to CTA (59). These positive results would propose a prospective trial to compare CEUS to advanced CT imaging as d-CTA in endoleak detection and characterization after EVAR. The results of such trial are much awaited from a research group who published their study protocol in 2018 (60).

The presented studies here, have their own limitations. The nature of a single-center, retrospective study will result in an inevitable selection bias. The cases enrolled were mainly complex endoleaks that were difficult to characterize, which may have impacted

the diagnostic accuracy of conventional t-CTA. The sample size in both studies is small which may have also influenced the results, although d-CTA being a recently adopted imaging technique at Houston Methodist Hospital limited the availability of patients having multiple modalities to compare without interim interventions. Furthermore, the comparison of radiation exposure between d-CTA and t-CTA is also limited due to the fact that the scans were acquired with different protocols and t-CTA imaging could have been further optimized to mitigate radiation burden which would have influenced our results. Nevertheless, we firmly believe this was necessary to highlight the magnitude of radiation burden using both modalities in a clinical setting and to provide a comparison with a standard technique. Further prospective studies are needed to clarify these points.

Based on our findings, despite being superior in endoleak characterization compared to the standard of care, t-CTA imaging - we suggest d-CTA to be the chosen modality in cases (1) when there is a known endoleak of unknown pathomechanism, (2) after previous embolization attempt, of evident aneurysm growth with (3) or without (4) any sign of endoleak, (5) as part of preoperative imaging prior to endoleak embolization, and (6) after complex endovascular procedures (such as F/B-EVAR) in the presence of endoleak.

Furthermore, recent advancements with endovascular devices and stent grafts have influenced the treatment of high-risk patients who otherwise are not fit for conventional open repair in aortic surgery (14, 15). More and more patients receive endovascular repair for aortic valve, ascending aorta, and aortic arch pathologies. Increased number of complex endovascular procedures in the aortic arch and ascending aorta will inevitably result in increased number of complications, therefore, adequate follow-up is mandatory after such procedures. Conventional CTA image quality in the proximal aorta is limited by cardiac motion (61), thus retrospective or prospectively triggered electrocardiography (ECG)-gated CTAs are performed to visualize the region of interest in a selected cardiac cycle (62). An advanced form of imaging is to combine the prospectively triggered ECG-gated technique with time-resolved, dynamic acquisition which can aid the diagnosis of graft-related complications in the proximal aorta, as we described it in our previous publication (63).

Finally, this technology is of great promise not only in endoleak characterization but in other dynamic disease processes, such as aortic intramural hematomas, dissections, arterio-venous malformations, or even in stroke imaging (64-68).

6. Conclusion:

6.1. Study I - Comparison of standard and dynamic computed tomography angiography in endoleak diagnosis

Based on our findings we conclude that dynamic computed tomography angiography imaging has better endoleak diagnosing capability as compared to standard triphasic computed tomography angiography when DSA was used as the reference standard.

There was no significant difference reported in radiation exposure between triphasic and dynamic CTA acquisitions.

In type II endoleak cases dynamic CTA identified more inflow vessels contributing to the pathomechanism of the endoleak as compared to triphasic CTA or DSA.

6.2. Study II - Quantitative approach to characterize endoleak types

Utilizing multiple CT scans, quantitative parameters such as Δ time to peak value demonstrated feasibility in objective endoleak analysis and can aid the differential diagnosis of endoleak types.

In type II endoleak cases dynamic CTA identified more inflow vessels contributing to the pathomechanism of the endoleak than DSA.

7. Summary:

The widespread use of EVAR has become apparent in the past decades. The favorable perioperative mortality rate (1.1% vs. 4.6% in Hungary and 0.6% vs. 3.8% in the United States) and the totally percutaneous nature of the procedure were the main driving factors of its success. However, major trials focusing on the long-term outcome of EVAR reported higher re-intervention rate with EVAR few years after the index procedure as compared to open repair. It is evident that as the number of EVARs grew over the years, a subsequent rise in the number of graft-related complications occurred. Thus, it was pertinent to adequately address the sequela of EVAR by utilizing advanced imaging techniques, such as dynamic, time-resolved CTA imaging.

In our study we describe the protocol developed for endoleak detection with d-CTA and the use of objective parameters such as Δ time to peak value in endoleak characterization. We found that d-CTA had a 100% accuracy to characterize endoleaks as compared to the standard of care, t-CTA, which showed a 73.7% accuracy, when DSA was the baseline reference.

Regarding the comparison of radiation exposure, the optimized d-CTA scans had a mean (±SD) dose-length product of 1445 (±550) and t-CTA had 1612 (±530) mGy*cm (p=0.255).

During a quantitative analysis of 23 patients, Δ TTP values (mean ±SD) between ROI_{aorta} and $ROI_{endoleak}$ were 1.8 ± 1.8 seconds for type I (n=4), 9.6 ± 3.5 seconds for type II (n=16), and 5.6 ± 1.3 seconds for type III endoleak (n=3), respectively. ΔTTP range was significantly narrower for type I endoleak as compared to type II endoleak.

In our studies d-CTA identified more target vessels contributing to type II endoleaks compared to other modalities (d-CTA, t-CTA, and DSA were 23, 17, and 16, respectively (p=0.009) and 33 vs. 21 vessels, p=0.010 (d-CTA vs DSA).

Our findings indicate that d-CTA was superior in endoleak characterization compared to t-CTA at an equivalent level of radiation. In type II endoleak cases d-CTA identified more vessels contributing to the endoleak as compared to t-CTA or DSA. Additionally, utilizing quantitative parameters such as ΔTTP can further aid differential diagnosis of endoleaks.

8. References:

1. Dubost C, Allary M, Oeconomos N. Resection of an aneurysm of the abdominal aorta: reestablishment of the continuity by a preserved human arterial graft, with result after five months. AMA Arch Surg. 1952;64(3):405-408.
2. Hertzer NR, Mascha EJ, Karafa MT, O'Hara PJ, Krajewski LP, Beven EG. (2002) Open infrarenal abdominal aortic aneurysm repair: the Cleveland Clinic experience from 1989 to 1998. J Vasc Surg. 2022;35(6):1145-1154.
3. Boyle JR, Mao J, Beck AW, Venermo M, Sedrakyan A, Behrendt CA, Szeberin Z, Eldrup N, Schermerhorn M, Beiles B, Thomson I, Cassar K, Altreuther M, Debus S, Johal AS, Watson S, Scali ST, Cromwell DA, Mani K. Editor's Choice - Variation in Intact Abdominal Aortic Aneurysm Repair Outcomes by Country: Analysis of International Consortium of Vascular Registries 2010 - 2016. Eur J Vasc Endovasc Surg. 2021;62(1):16-24.
4. Chaikof EL, Dalman RL, Eskandari MK, Jackson BM, Lee WA, Mansour MA, Mastracci TM, Mell M, Murad MH, Nguyen LL, Oderich GS, Patel MS, Schermerhorn ML, Starnes BW. The Society for Vascular Surgery practice guidelines on the care of patients with an abdominal aortic aneurysm. J Vasc Surg. 2018;67(1):2-77 e2.
5. Wanhainen A, Verzini F, Van Herzeele I, Allaire E, Bown M, Cohnert T, Dick F, van Herwaarden J, Karkos C, Koelemay M, Kölbel T, Loftus I, Mani K, Melissano G, Powell J, Szeberin Z, Esvs Guidelines Committee, de Borst GJ, Chakfe N, Debus S, Hinchliffe R, Kakkos S, Koncar I, Kolh P, Lindholt JS, de Vega M, Vermassen F, Document Reviewers, Björck M, Cheng S, Dalman R, Davidovic L, Donas K, Earnshaw J, Eckstein HH, Golledge J, Haulon S, Mastracci T, Naylor R, Ricco JB, Verhagen H. Editor's Choice - European Society for Vascular Surgery (ESVS) 2019 Clinical Practice Guidelines on the Management of Abdominal Aorto-iliac Artery Aneurysms. Eur J Vasc Endovasc Surg. 2019;57(1):8-93.
6. Műtéti statisztika 2021, Semmelweis Egyetem, Érsebészeti és Endovaszkuláris Tanszék, Budapest 2021.
7. Hidi L, Pál D, Boros AM, Kováts T, Menyhei G, Szeberin Z. Infrarenalis aortaaneurysma-műtétek országos eredményeinek elemzése a Nemzeti

Érsebészeti Regiszter alapján (2010–2019) [Analysis of data from the National Vascular Registry on infrarenal aortic aneurysms (2010–2019)]. Orv Hetil, 2021;162(31):1233-1243.

8. Berczeli M, Osztrogonácz P, Hidi L, Szeberin Z. Percutan endovascularis aortarekonstrukcióval szerzett kezdeti tapasztalataink. Orv Hetil. 2022;163(33):1318-1323.
9. Nelson PR, Kracjer Z, Kansal N, Rao V, Bianchi C, Hashemi H, Jones P, Bacharach JM. A multicenter, randomized, controlled trial of totally percutaneous access versus open femoral exposure for endovascular aortic aneurysm repair (the PEVAR trial). J Vasc Surg. 2014;59(5):1181-1193.
10. Cao Z, Wu W, Zhao K, Zhao J, Yang Y, Jiang C, Zhu R. Safety and Efficacy of Totally Percutaneous Access Compared with Open Femoral Exposure for Endovascular Aneurysm Repair: A Meta-analysis. J Endovasc Ther. 2017;24(2):246-253.
11. De Bruin JL, Baas AF, Buth J, Prinssen M, Verhoeven EL, Cuypers PW, van Sambeek MR, Balm R, Grobbee DE, Blankensteijn JD, DREAM Study Group. Long-term outcome of open or endovascular repair of abdominal aortic aneurysm. N Engl J Med. 2010;362(20):1881-9.
12. Powell JT, Sweeting MJ, Ulug P, Blankensteijn JD, Lederle FA, Becquemin JP, Greenhalgh RM, EVAR-1, DREAM, OVER and ACE Trialists. Meta-analysis of individual-patient data from EVAR-1, DREAM, OVER and ACE trials comparing outcomes of endovascular or open repair for abdominal aortic aneurysm over 5 years [published correction appears in Br J Surg. 2018;105(9):1222]. Br J Surg. 2017;104(3):166-178.
13. Lederle FA, Kyriakides TC, Stroupe KT, Freischlag JA, Padberg FT Jr, Matsumura JS, Huo Z, Johnson GR, OVER Veterans Affairs Cooperative Study Group. Open versus Endovascular Repair of Abdominal Aortic Aneurysm. N Engl J Med. 2019;380(22):2126-2135.
14. Roselli EE, Idrees J, Greenberg RK, Johnston DR, Lytle BW. Endovascular stent grafting for ascending aorta repair in high-risk patients. J Thorac Cardiovasc Surg. 2015;149(1):144-51.

15. Tsilimparis N, Debus ES, Oderich GS, Haulon S, Terp KA, Roeder B, Detter C, Kölbel T. International experience with endovascular therapy of the ascending aorta with a dedicated endograft. J Vasc Surg. 2016;63(6):1476-82.
16. Kärkkäinen JM, Tenorio ER, Jain A, Mendes BC, Macedo TA, Pather K, Gloviczki P, Oderich GS. Outcomes of target vessel endoleaks after fenestrated-branched endovascular aortic repair. J Vasc Surg. 2020;72(2):445-455.
17. Andersson M, Sandström C, Stackelberg O, Lundqvist R, Nordanstig J, Jonsson M, Roy J, Andersson M, Hultrgren R, Roos H. Editor's Choice - Structured Computed Tomography Analysis Can Identify the Majority of Patients at Risk of Post-Endovascular Aortic Repair Rupture. Eur J Vasc Endovasc Surg. 2022;64(2-3):166-174.
18. Lehmkuhl L, Andres C, Lücke C, Hoffmann J, Foldyna B, Grothoff M, Nitzsche S, Schmidt A, Ulrich M, Scheinert D, Gutberlet M. Dynamic CT angiography after abdominal aortic endovascular aneurysm repair: influence of enhancement patterns and optimal bolus timing on endoleak detection. Radiology. 2013;268(3):890-899.
19. Belkin N, Jackson BM, Foley PJ, Damrauer SM, Kalapatapu V, Golden MA, Fairman RM, Wang JG. The use of intravascular ultrasound in the treatment of type B aortic dissection with thoracic endovascular aneurysm repair is associated with improved long-term survival. J Vasc Surg. 2020;72(2):490-497.
20. Kinner S, Eggebrecht H, Maderwald S, Barkhausen J, Ladd SC, Quick HH, Hunold P, Vogt FM. Dynamic MR angiography in acute aortic dissection. J Magn Reson Imaging. 2015;42(2):505-514.
21. Azarine A, Garçon P, Stansal A, Canepa N, Angelopoulos G, Silvera S, Sidi D, Marteau V, Zins M. Four-dimensional Flow MRI: Principles and Cardiovascular Applications. Radiographics. 2019;39(3):632-648
22. Sommer WH, Becker CR, Haack M, Rubin GD, Weidenhagen R, Schwarz F, Nikolau K, Reiser MF, Johnson TR, Clevert DA. Time-resolved CT angiography for the detection and classification of endoleaks. Radiology. 2012;263(3):917-926.
23. Hou K, Zhu T, Zhang W, Zeng M, Guo D, Fu W, Si. Dynamic Volumetric Computed Tomography Angiography Is a Preferred Method for Unclassified

Endoleaks by Conventional Computed Tomography Angiography After Endovascular Aortic Repair. J Am Heart Assoc. 2019;8(8):e012011.

24. Berczeli M, Chinnadurai P, Legeza P, Peden EK, Bavare CS, Chang SM, Lumsden AB. (2022) Dynamic, Time-Resolved CT Angiography After EVAR: (2022) A Quantitative Approach to Accurately Characterize Aortic Endoleak Type and Identify Inflow Vessels [published online ahead of print, 2022 Jan 23]. J Endovasc Ther. 2022 doi:10.1177/15266028211070970
25. Madigan MC, Singh MJ, Chaer RA, Al-Khoury GE, Makaroun MS. Occult type I or III endoleaks are a common cause of failure of type II endoleak treatment after endovascular aortic repair. J Vasc Surg. 2019;69(2):432-439.
26. Eden CL, Long GW, Major M, Studzinski D, Brown OW. Type II endoleak with an enlarging aortic sac after endovascular aneurysm repair predisposes to the development of a type IA endoleak. J Vasc Surg. 2020;72(4):1354-1359.
27. Koike Y, Ishida K, Hase S, Kobayashi Y, Nishimura JI, Yamasaki M, Hosaka N. Dynamic volumetric CT angiography for the detection and classification of endoleaks: application of cine imaging using a 320-row CT scanner with 16-cm detectors. J Vasc Interv Radiol. 2014;25(8):1172-1180.
28. Lehmkuhl L, Andres C, Lücke C, Foldyna B, Grothoff M, Scheinert D, Nitzsche S, Gutberlet M. Dynamic CT angiography after abdominal aortic endovascular aneurysm repair: differences in contrast agent dynamics in the aorta and endoleaks--preliminary results. J Vasc Interv Radiol. 2012;23(6):744-750.
29. Berczeli M, Lumsden AB, Chang SM, Bavare CS, Chinnadurai P. Dynamic, Time-Resolved Computed Tomography Angiography Technique to Characterize Aortic Endoleak Type, Inflow and Provide Guidance for Targeted Treatment. J Endovasc Ther. 2022;29(1):11-22.
30. Berczeli M, Chinnadurai P, Chang SM, Lumsden AB. Time-Resolved, Dynamic Computed Tomography Angiography for Characterization of Aortic Endoleaks and Treatment Guidance via 2D-3D Fusion-Imaging. J Vis Exp. 2021;(178):10.3791/62958.
31. Berczeli M, Chinnadurai P, Osztrogonácz P, Peden EK, Bavare CS, Sótonyi P, Chang SM, Lumsden AB. Dynamic Computed Tomography Angiography is More Accurate in Diagnosing Endoleaks than Standard Triphasic Computed

Tomography Angiography and Enables Targeted Embolization. Ann Vasc Surg. 2023;88:318-326.

32. Abi-Jaoudeh N, Kobeiter H, Xu S, Wood BJ. Image fusion during vascular and nonvascular image-guided procedures. Tech Vasc Interv Radiol. 2013;16(3):168-176.
33. Varnavas A, Carrell T, Penney G. Fully automated 2D-3D registration and verification. Med Image Anal. 2015;26(1):108-119.
34. Jones DW, Stangenberg L, Swerdlow NJ, Alef M, Lo R, Shuja F, Schermerhorn ML. Image Fusion and 3-Dimensional Roadmapping in Endovascular Surgery. Ann Vasc Surg. 2018;52:302-311.
35. Cieri E, De Rango P, Isernia G, Simonte G, Ciucci A, Parlani G, Verzini F, Cao P. Type II endoleak is an enigmatic and unpredictable marker of worse outcome after endovascular aneurysm repair. J Vasc Surg. 2014;59(4):930-937.
36. Lalys F, Daoudal A, Gindre J, Göksu C, Lucas A, Kaladji A. Influencing factors of sac shrinkage after endovascular aneurysm repair. J Vasc Surg. 2017;65(6):1830-1838.
37. Sarac TP, Gibbons C, Vargas L, Liu J, Srivastava S, Bena J, Mastracci T, Kashyap VS, Clair D. Long-term follow-up of type II endoleak embolization reveals the need for close surveillance. J Vasc Surg. 2012;55(1):33-40.
38. Aziz A, Menias CO, Sanchez LA, Picus D, Saad N, Rubin BG, Curci JA, Geraghty PJ. Outcomes of percutaneous endovascular intervention for type II endoleak with aneurysm expansion. J Vasc Surg. 2012;55(5):1263-1267.
39. Sidloff DA, Stather PW, Choke E, Bown MJ, Sayers RD. Type II endoleak after endovascular aneurysm repair. Br J Surg. 2013;100(10):1262-1270.
40. Ultee KHJ, Büttner S, Huurman R, Goncalves BF, Hoeks SE, Bramer WM, Schermerhorn ML, Verhagen HJM. Editor's Choice - Systematic Review and Meta-Analysis of the Outcome of Treatment for Type II Endoleak Following Endovascular Aneurysm Repair. Eur J Vasc Endovasc Surg. 2018;56(6):794-807.
41. Seike Y, Matsuda H, Shimizu H, Ishimaru S, Hoshina K, Michihata N, Yasunaga H, Komori K, Japanese Committee for Stentgraft Management (JACSM). Nationwide Analysis of Persistent Type II Endoleak and Late Outcomes of

Endovascular Abdominal Aortic Aneurysm Repair in Japan: A Propensity-Matched Analysis. Circulation. 2022;145(14):1056-1066.

42. Wu WW, Swerdlow NJ, Dansey K, Shuja F, Wyers MC, Schermerhorn ML. (2021) Surgical treatment patterns and clinical outcomes of patients treated for expanding aneurysm sacs with type II endoleaks after endovascular aneurysm repair. J Vasc Surg. 2022;73(2):484-493.
43. Berczeli M, Csobay-Novák C, Oláh Z, Sótonyi P. Multistage Endovascular Management of an Aortic Aneurysm Rupture into the Retroaortic Left Renal Vein. Ann Vasc Surg. 2021;73:509.
44. Sommer WH, Clevert DA, Bamberg F, Helck A, Albrecht E, Reiser MF, Becker CR, Nikolaou K. Time-resolved computed tomography imaging of the aorta: a feasibility study. J Thorac Imaging. 2010;25(2):161-167.
45. Apfaltrer G, Lavra F, Schoepf UJ, Scarabello M, Yamada R, van Assen M, Varga-Szemes A, Jacobs BE, Bauer MJ, Greenberg WT, Guimaraes M, Saba L, De Cecco CN. Quantitative analysis of dynamic computed tomography angiography for the detection of endoleaks after abdominal aorta aneurysm endovascular repair: A feasibility study. PLoS One. 2021;16(1): e0245134.
46. Charalambous S, Perisinakis K, Kontopodis N, Kontopodis N, Papadakis AE, Galanakis N, Kehagias E, Matthaiou N, Maris TG, Ioannou CV, Tsetis D. Discrimination of High-Risk Type-2 Endoleak after Endovascular Aneurysm Repair through CT Perfusion: A Feasibility Study. J Vasc Interv Radiol. 2021; 32(6):807-812.
47. Iwakoshi S, Ogawa Y, Dake MD, Ono Y, Higashihara H, Ikoma A, Nakai M, Taniguchi T, Ogi T, Kawada H, Tamura A, Ieko Y, Tanaka R, Sohgawa E, Nagatomi S, Woodhams R, Ikeda O, Mori K, Nishimaki H, Koizumi J, Senokuchi T, Hagihara M, Shimohira M, Takasugi S, Imaizumi A, Higashiura W, Sakaguchi S, Ichihashi S, Inoue T, Inoue T, Kichikawa K. Outcomes of embolization procedures for type II endoleaks following endovascular abdominal aortic repair. J Vasc Surg. 2022;S0741-5214(22)02099-7. doi: 10.1016/j.jvs.2022.07.168.
48. Charitable JF, Patalano PI, Garg K, Garg K, Maldonado TS, Jacobowitz GR, Rockman CB, Veith FJ, Cayne NS. Outcomes of translumbar embolization of type

II endoleaks following endovascular abdominal aortic aneurysm repair. J Vasc Surg. 2021;74(6):1867-1873.

49. Spenkelink IM, Heidkamp J, Fütterer JJ, Rovers MM. Image-guided procedures in the hybrid operating room: a systematic scoping review. PLoS One. 2022;17(4): e0266341.
50. Hertault A, Maurel B, Sobocinski J, Gonzalez TM, Le Roux M, Azzaoui R, Midulla M, Haulon S. (2014) Impact of hybrid rooms with image fusion on radiation exposure during endovascular aortic repair. Eur J Vasc Endovasc Surg. 2014; 48(4):382– 390.
51. Ahmad W, Hasselmann HC, Galas N, Majd P, Brunkwall S, Brunkwall JS. Image fusion using the two-dimensional-three-dimensional registration method helps reduce contrast medium volume, fluoroscopy time, and procedure time in hybrid thoracic endovascular aortic repairs. J Vasc Surg. 2019;69(4):1003-1010.
52. Maurel B, Martin-Gonzalez T, Chong D, Irwin A, Guimbretiere G, Davis M, Mastracci TM. A prospective observational trial of fusion imaging in infrarenal aneurysms. J Vasc Surg. 2018;68(6):1706-1713.
53. Zaarour Y, Kobeiter H, Derbel H, Vitellius M, Ridouani F, You K, Touma J, Cochennec F, Desgranges P, Tacher V. Immediate and 1-year success rate of type 2 endoleak treatment using three-dimensional image fusion guidance. Diagn Interv Imaging. 2020;101(9):589-598.
54. Yu H, Desai H, Isaacson AJ, Dixon RG, Farber MA, Burke CT. Comparison of Type II Endoleak Embolizations: Embolization of Endoleak Nidus Only versus Embolization of Endoleak Nidus and Branch Vessels. J Vasc Interv Radiol. 2017;28(2):176-184.
55. Bredahl KK, Taudorf M, Lönn L, Vogt KC, Sillesen H, Eiberg JP. Contrast Enhanced Ultrasound Can Replace Computed Tomography Angiography for Surveillance After Endovascular Aortic Aneurysm Repair. Eur J Vasc Endovasc Surg. 2016;52(6):729-734.
56. Mirza TA, Karthikesalingam A, Jackson D, Walsh SR, Holt PJ, Hayes PD, Boyle JR. Duplex ultrasound and contrast-enhanced ultrasound versus computed tomography for the detection of endoleak after EVAR: systematic review and bivariate meta-analysis. Eur J Vasc Endovasc Surg. 2010;39(4):418-428.

57. Perini P, Sediri I, Midulla M, Delsart P, Mouton S, Gautier C, Pruvo JP, S Haulon. Single-centre prospective comparison between contrast-enhanced ultrasound and computed tomography angiography after EVAR. Eur J Vasc Endovasc Surg. 2011;42(6):797-802.
58. Guo Q, Zhao J, Huang B, Yuan D, Yang Y, Zeng G, Xiong F, Du X. A Systematic Review of Ultrasound or Magnetic Resonance Imaging Compared with Computed Tomography for Endoleak Detection and Aneurysm Diameter Measurement After Endovascular Aneurysm Repair. J Endovasc Ther. 2016;23(6):936-943.
59. Lowe C, Abbas A, Rogers S, Smith L, Ghosh J, McCollum C. Three-dimensional contrast-enhanced ultrasound improves endoleak detection and classification after endovascular aneurysm repair. J Vasc Surg. 2017;65(5):1453-1459.
60. Roy IN, Chan TY, Czanner G, Wallace S, Vallabhaneni SR. Prospective, single UK centre, comparative study of the predictive values of contrast-enhanced ultrasound compared to time-resolved CT angiography in the detection and characterisation of endoleaks in high-risk patients undergoing endovascular aneurysm repair surveillance: a protocol. BMJ Open. 2018;8(4): e020835.
61. de Beaufort HW, Nauta FJ, Conti M, Cellitti E, Trentin C, Faggiano E, van Bogerijen GHW, Figueroa CA, Moll FL, van Herwaarden JA, Auricchio F, Trimarchi S. Extensibility and Distensibility of the Thoracic Aorta in Patients with Aneurysm. Eur J Vasc Endovasc Surg. 2017;53(2):199-205.
62. Csobay-Novák C, Fontanini DM, Szilágyi BR, Szeberin Z, Szilveszter B, Maurovich-Horvat P, Hüttl K, Sótonyi P. Thoracic aortic strain can affect endograft sizing in young patients. J Vasc Surg. 2015;62(6):1479-1484.
63. Berczeli M, Chinnadurai P, Ramirez-Giraldo JC, Garami Z, Lumsden AB, Atkins MD, Chang SM. Time-resolved, Cardiac-gated Computed Tomography After Endovascular Ascending Aortic and Arch Repair. Ann Thorac Surg. 2022;113(5):1685-1691.
64. Berczeli M, Chang SM, Lumsden AB, Chinnadurai P. Imaging aortic intramural hematoma with blood pools using time-resolved, dynamic computed tomography angiography. J Vasc Surg. 2022;76(4):1087-1088.

65. Meinel FG, Nikolaou K, Weidenhagen R, Hellbach K, Helck A, Bamberg F, Reiser MF, Sommer WH. Time-resolved CT angiography in aortic dissection. Eur J Radiol. 2012;81(11):3254-3261.
66. Meyer M, Geiger N, Benck U, Rose D, Sudarski S, Ong MM, Schoenberg SO, Henzler T. Imaging of Patients with Complex Hemodialysis Arterio-Venous Fistulas using Time-Resolved Dynamic CT Angiography: Comparison with Duplex Ultrasound. Sci Rep. 2017;7(1):12563.
67. Shankar JJ, Lum C, Chakraborty S, Dos Santos M. Cerebral vascular malformations: Time-resolved CT angiography compared to DSA. Neuroradiol J. 2015;28(3):310-315.
68. Menon BK, d'Esterre CD, Qazi EM, Almekhlafi M, Hahn L, Demchuk AM, Goyal M. Multiphase CT Angiography: A New Tool for the Imaging Triage of Patients with Acute Ischemic Stroke. Radiology. 2015;275(2):510-520.

9. Bibliography of the candidate's publications:

9.1. Publications directly related to thesis:

Berczeli M, Chang SM, Lumsden AB, Chinnadurai P. Imaging aortic intramural hematoma with blood pools using time-resolved, dynamic computed tomography angiography. J Vasc Surg. 2022;76(4):1087-1088. **IF: 4.860**

Berczeli M, Chinnadurai P, Osztrogonácz P, Peden EK, Bavare CS, Sótonyi P, Chang SM, Lumsden AB. Dynamic Computed Tomography Angiography is More Accurate in Diagnosing Endoleaks than Standard Triphasic Computed Tomography Angiography and Enables Targeted Embolization. Ann Vasc Surg. 2023;88:318-326. **IF: 1.607**

Berczeli M, Chinnadurai P, Legeza P, Peden EK, Bavare CS, Chang SM, Lumsden AB. (2022) Dynamic, Time-Resolved CT Angiography After EVAR: (2022) A Quantitative Approach to Accurately Characterize Aortic Endoleak Type and Identify Inflow Vessels [published online ahead of print, 2022 Jan 23]. J Endovasc Ther. 2022 doi:10.1177/15266028211070970 **IF:3.089**

Berczeli M, Chinnadurai P, Ramirez-Giraldo JC, Garami Z, Lumsden AB, Atkins MD, Chang SM. Time-resolved, Cardiac-gated Computed Tomography After Endovascular Ascending Aortic and Arch Repair. Ann Thorac Surg. 2022;113(5):1685-1691. **IF:5.113**

Berczeli M, Chinnadurai P, Chang SM, Lumsden AB. Time-Resolved, Dynamic Computed Tomography Angiography for Characterization of Aortic Endoleaks and Treatment Guidance via 2D-3D Fusion-Imaging. J Vis Exp. 2021; (178):10.3791/62958. **IF:1.424**

Berczeli M, Lumsden AB, Chang SM, Bavare CS, Chinnadurai P. Dynamic, Time-Resolved Computed Tomography Angiography Technique to Characterize Aortic Endoleak Type, Inflow and Provide Guidance for Targeted Treatment. J Endovasc Ther. 2022;29(1):11-22. **IF:3.089**

Berczeli M, Csobay-Novák C, Oláh Z, Sótonyi P. Multistage Endovascular Management of an Aortic Aneurysm Rupture into the Retroaortic Left Renal Vein. Ann Vasc Surg. 2021;73:509. e11-509.e14. **IF: 1.607**

9.2. Publications directly not related to thesis:

Berczeli M, P Osztrogonácz, L Hidi, and Z Szeberin. (2022) Percutan Endovascularis Aortarekonstrukcióval Szerzett Kezdeti Tapasztalataink. ORVOSI HETILAP 163 (33): 1318–1323. **IF:0.707**

Berczeli M., P. Chinnadurai, R.G. McFall, O. Diaz, and A.B. Lumsden. (2022) Endovascular Treatment of Pancreaticoduodenal Aneurysm with Braided Stent-Assisted Coil Embolization Using Intraoperative Cone-Beam Computed Tomography Guidance. JOURNAL OF VASCULAR SURGERY CASES AND INNOVATIVE TECHNIQUES 8 (2): 265–270. **IF:-**

Berczeli M and David Garbaisz. (2022) Total Hip AND Femoral Artery Replacement. EUROPEAN JOURNAL OF VASCULAR AND ENDOVASCULAR SURGERY 2022;64(2-3):216 **IF: 6.427**

Berczeli M, Chinnadurai P, Veress DS, Diaz O, Bavare CS and Lumsden AB. (2022) Added Value of Selective Intra-Arterial Cone-Beam CT Angiography in the Management of Visceral Artery Aneurysms." JOURNAL OF ENDOVASCULAR THERAPY In press: 152660282211185. **IF:3.089**

Berczeli M, Gavin W. Britz, Thomas Loh, and Alan B. Lumsden. (2022) Telerobotic Endovascular Interventions and Their Potential for Cerebrovascular Treatment. TEXAS HEART INSTITUTE JOURNAL 49 (2). **IF:1.103**

Berczeli M, Chinnadurai P, Legeza PT, Britz GW and Lumsden AB. (2022) Transcarotid Access for Remote Robotic Endovascular Neurointerventions: A Cadaveric Proof-of-Concept Study. NEUROSURGICAL FOCUS 52 (1). **IF:4.332**

Hendricks W, Mecca J, Rahimi M, Rojo MR, Von Ballmoos MWC, McFall RG, Haddad P, **Berczeli M**, Sinha K, Barnes RG., Peden EK., Lumsden AB., MacGillivray TE, Corr

S. (2022) Evaluation of a Novel System for RFID Intraoperative Cardiovascular Analytics. IEEE JOURNAL OF TRANSLATIONAL ENGINEERING IN HEALTH AND MEDICINE-JTEHM 10: 1–9. **IF:2.890**

Legeza, PT, Lettenberger AB, Murali B, Johnson LR, **Berczeli M,** Byrne MD, Britz G, O'Malley MK and Lumsden AB. (2022) Evaluation of Robotic-Assisted Carotid Artery Stenting in a Virtual Model Using Motion-Based Performance Metrics. JOURNAL OF ENDOVASCULAR THERAPY. **IF:3.089**

Sinha, K., **Berczeli M,** Lumsden AB, and Roy TL. (2022) Imaging: New Frontiers in Vascular Training. Methodist DeBakey Cardiovascular Journal 18 (3): 39–48. **IF:-**

Gyánó, M., **Berczeli M**, Csobay-Novák C, Szöllősi D, Óriás VI, Góg I, Kiss JP, Veres DS, Szigeti K, Osváth S, Pataki Á, Juhász V, Oláh Z, Sótonyi P, Nemes B. (2021) Digital Variance Angiography Allows about 70% Decrease of DSA-Related Radiation Exposure in Lower Limb X-Ray Angiography. SCIENTIFIC REPORTS 11 (1). **IF:4.997**

Patelis N, Bisdas T, Jing Z, Feng J, Trenner M, Tri Nugroho N, Ocke Reis PE, Elkouri S, Lecis A, Karam L, Roux DL, Ionac M, **Berczeli M**, Jongkind V, Yeung KK, Katsargyris A, Avgerinos E, Moris D, Choong A, Ng JJ, Cvjetko I, Antoniou GA, Ghibu P, Svetlikov A, Pedrajas FG, Ebben H, Stepak H, Chornuy A, Kostiv S, Ancetti S, Tadayon N, Mekkar A, Magnitskiy L, Fidalgo-Domingos L, Matheiken S, Sarutte Rosello ES, Isik A, Kirkilesis G, Kakavia K, Georgopoulos S. (2021) Dataset of the Vascular E-Learning during the COVID-19 Pandemic (EL-COVID) Survey. DATA IN BRIEF 38. **IF:-**

Patelis N, Bisdas T, Jing Z, Feng J, Trenner M, Tri Nugroho N, Ocke Reis PE, Elkouri S, Lecis A, Karam L, Roux DL, Ionac M, **Berczeli M**, Jongkind V, Yeung KK, Katsargyris A, Avgerinos E, Moris D, Choong A, Ng JJ, Cvjetko I, Antoniou GA, Ghibu P, Svetlikov A, Pedrajas FG, Ebben H, Stepak H, Chornuy A, Kostiv S, Ancetti S, Tadayon N, Mekkar A, Magnitskiy L, Fidalgo-Domingos L, Matheiken S, Sarutte Rosello ES, Isik A, Kirkilesis G, Kakavia K, Georgopoulos S (2021) Vascular E-Learning During the COVID-19 Pandemic: The EL-COVID Survey. ANNALS OF VASCULAR SURGERY 77: 63–70. **IF:1.607**

Berczeli M, Oláh Z, Szatai L, Daróczi L, Sótonyi P. (2020) Rupturált Óriás Thoracoabdominalis Aortaaneurysma Sikeres Kezelése Két Lépésben = Successful Two-Step Treatment of a Ruptured Giant Thoracoabdominal Aortic Aneurysm. ORVOSI HETILAP 161 (7): 269–274. **IF:0.707**

Gyánó, M, Csobay-Novák C, **Berczeli M**, Góg I, Kiss JP, Szigeti K, Osváth S, Nemes B. (2020) Initial Operating Room Experience with Digital Variance Angiography in Carbon Dioxide-Assisted Lower Limb Interventions: A Pilot Study. CARDIOVASCULAR AND INTERVENTIONAL RADIOLOGY 43 (8): **IF:2.797**

Pál, D, Szilágyi B, **Berczeli M**, Szalay CsI, Sárdy B, Oláh Z, Székely T, Rácz G, Banga P, Czinege Z, Sótonyi P. (2020) Ruptured Aortic Aneurysm and Dissection Related Death: An Autopsy Database Analysis. PATHOLOGY AND ONCOLOGY RESEARCH 26 (4): 2391–2399. **IF:2.874**

Szilágyi B, **Berczeli M**, Lovas A, Oláh Z, Törő K, Sótonyi P. (2020) The Effects of Changing Meteorological Parameters on Fatal Aortic Catastrophes. BMC CARDIOVASCULAR DISORDERS 20 (1). **IF:2.174**

Tóth-Vajna Z, Tóth-Vajna G, Gombos Z, Szilágyi B, Járai Z, **Berczeli M**, Sótonyi P. (2019) Screening of Peripheral Arterial Disease in Primary Health Care. VASCULAR HEALTH AND RISK MANAGEMENT 15: 355–363. **IF:-**

Berczeli M, Szilágyi B, Lovas A, Pál D, Oláh Z, Törő K, Sótonyi P. (2018) Meteorológiai Paraméterek Változásának Hatása a Halálos Kimenetelű Aortaaneurysma-Rupturákra. ORVOSI HETILAP 159 (37): 1501–1505. **IF:0.707**

Nagy Z, Oláh Z, Kókai J, Molnár AB, Laczkó Á, Szabó GV, Juhász V, Garbaisz D, **Berczeli M**, Sztupinszky Z, Szeberin Z (2017) Homograftok Szerepe Az Alsó Végtagi Érrekonstrukciókban. MAGYAR SEBÉSZET 70 (1): 5–12. **IF:-**

10. Acknowledgements:

First of all, I wish to express my deepest gratitude to my family and friends who supported me and continue to do so in my everyday life.

This thesis is based on multiple publications which were performed at the Department of Cardiovascular Surgery of Houston Methodist Hospital and at the Department of Vascular and Endovascular Surgery of Semmelweis University. This thesis would not have happened without the support of kind colleagues both in Hungary and overseas to whom I would like to extend my sincere thanks.

I am absolutely grateful to my supervisor, Prof. Péter Sótonyi who helped me in many ways and encouraged me when I needed the most. I am thankful to him that I could turn to him whenever it was necessary or unnecessary.

I am thankful for the blessed time I spent in the Mecca of Aortic Surgery. This could not have happened without the help of Dr Zsolt Garami and Prof. Alan Lumsden. Over and above, Prof. Lumsden mentored me and influenced my mindset both in professional and personal ways.

My greatest appreciation also goes to Dr Ponraj Chinnadurai, who guided me, taught me, spent most of his Fridays educating me, and who implanted the idea of surgical imaging in my head. He was not only fundamental in my success but became a friend of mine over time, too.

I am also thankful to Dr Su Min Chang for his important aspects in imaging, critique, encouragement, and sharing his point of view throughout our cooperation.

I am also very grateful to Dr Zoltán Szeberin – my mentor in training - and Dr Péter Banga for their continuous help in supporting my projects both scientifically and clinically.

I would also like to thank the support of the imaging group at the Heart and Vascular Center in Hungary with whom together we initiated dynamic CT imaging at Semmelweis University.

Last but not least, I am grateful to Alexandra Bakó for lecturing this work and all the reviewers for their time and impact that significantly improved this thesis.